Texture Analysis of Microscopy Images from Power Transformer Cellulose Insulation for Aging Condition Assessment

by

Nathan Dale Jacob

A Thesis submitted to the Faculty of Graduate Studies of
The University of Manitoba
in partial fulfillment of the requirements of the degree of

Doctor of Philosophy

Department of Electrical and Computer Engineering
University of Manitoba
Winnipeg, Canada

Abstract

Electrical paper insulation used in power transformers thermally deteriorates during the normal transformer operation. When this deterioration becomes significant, tensile strength is reduced, and the risk for insulation failure is increased. The most accurate method for paper condition assessment is the degree of polymerization (DP) measurement, where a sample of paper is removed from the transformer for chemical analysis. However, the quantity of paper required for DP measurement is often considered too invasive. In this research, methods for texture analysis on microscopic images of thermally aged insulation paper, is presented as an alternative approach for condition assessment.

An experimental setup was developed to artificially age oil-impregnated Kraft paper samples. The samples were thermally stressed in an oven at temperatures above those normally present in power transformers, to produce a sample set with varying levels of insulation deterioration.

Microscopy images of the paper samples were analyzed using two texture analysis methods. The first method is a statistical-based texture analysis method called the spatial grey level dependence method (SGLDM). SGLDM converts images into matrices containing information about the statistical variation of pixel grey-level intensities in an image. Mathematical operators applied to the SGLDM are used to extract 22 statistical texture features for each sample image. The second method uses a two-dimensional Wavelet transform to extract detail information from Wavelet decomposition coefficient matrices. The Wavelet method is applied recursively, with four decompositions, producing a total of 12 Wavelet texture features per sample image.

Analysis of the microscopy images obtained from thermally aged samples show that thermal deterioration of the insulation paper produces changes in the surface morphology and physical structure. These changes are detectable by the texture features extracted from the SGLDM and Wavelet texture analysis. Correlations between texture features and DP measurements performed on the paper samples are analyzed, and statistical classification is

performed on the feature set to demonstrate that differentiation between oil-impregnated paper samples with different levels of thermal degradation is reliable with low error rates. Therefore, development of a practical method to assess condition of oil-impregnated paper insulation using optical microscopy and texture analysis is promising.

Acknowledgements

Firstly, I would like to thank my advisors Dr. Behzad Kordi and Dr. Sherif Sherif for their support and guidance through this thesis. I also extend thanks to the other members of my examining committee, Dr. David Swatek and Dr. Mazdak Khajehpour. Secondly, I acknowledge Manitoba Hydro for financial support.

I have been fortunate to have had good and generous mentors in my career thus far, in particular I thank David Swatek for providing me motivation throughout this pursuit, and Bill McDermid who has spurred my interest in this technical area of work. I also thank my colleagues at Manitoba Hydro's Insulation Engineering and Testing Department for their encouragement through this long endeavor.

I am thankful to my parents for all they've invested in me over the years. My mother has given me great encouragement in all my academic and professional goals. Sadly, I regret not being able to have the opportunity to celebrate this accomplishment with my father. More than anything, he taught me the importance of hard work, and without which, as my personal philosophy, I would not have achieved this goal.

Lastly, for her endless support and caring, I am thankful to my loving wife Delia. I am fortunate to have you as my advisor, my friend, and the love of my life.

Table of Contents

List of Figures

List of Tables

Chapter 1

Introduction

1.1 Problem Statement and Motivation

Together with switchgear and generators, power transformers are one of three main components used for the transmission of electrical energy [1]. A photograph of a power transformer is shown in Fig. 1.1. The main purpose of power transformers in the electrical transmission system is to convert voltage from one magnitude level to another. Power transformers are highly reliable apparatus with life expectancies that can exceed 40-years when operated under normal loading conditions and system voltages [2–4]. However, shortened life spans occur when power transformers are operated at or near their full load rating continuously. Aging models used within the utility industry predict end-of-life criteria may be reached in as little 20.5 years (180,000 hours) [2]. Therefore utilities which are forced to operate at full load continuously should expect life spans much shorter than 40-years. Some utility companies in Asia report that less than 5% of their 110 kV class power transformers achieve an operational life of 30 years and less than 1% reach 40 years. [5]. For utilities, forced outages of power transformers due to insulation failure is costly. Outage durations can be long and the replacement costs are high; typically in the order of $1 million dollars. There is also the

Fig. 1.1. A power transformer, courtesy of Manitoba Hydro.

potential for legal and financial implications due to customer service disruptions as well as potential for safety risks to field workers or the public when failures are explosive.

In most power transformers, the electrical insulation system is composed of mineral oil and oil-impregnated paper, and the most common type of paper used is a cellulose based paper called kraft paper. During normal, in-service operation of the transformer, thermal, electrical, and chemical stresses continually degrade these materials [2, 6]. With regular planned maintenance, the transformer insulating oil can be replaced or reprocessed to restore its original properties. For the kraft paper the effects of degradation are permanent. The most common cause of power transformer failure occurs when the kraft insulation paper degrades to the point that its mechanical properties are inadequate to sustain isolation between the transformer winding turns.

Existing methods for evaluating the condition transformer paper insulation include detection of chemical markers found in oil samples taken from the transformer [7], or by tests performed directly on paper samples removed from the transformer, such as the degree of polymerization(DP) measurement [8, 9]. Effective assessment of the paper condition based on detection of chemical markers in the insulating oil are hindered by dilution. The relative concentrations of these markers in the overall oil volume may be indicative of

distributed defects where the paper still has a considerable amount of remaining life, or may be indicative of an acute defect where the paper is close to failure. The degree of polymerization test which is performed with samples of paper removed from the transformer is problematic because the sample size required for analysis are large enough to be considered invasive and potentially damaging to the power transformer.

Previous research has shown that the deterioration of kraft insulation paper in power transformers manifests morphological changes to the microscopic structure of the insulation paper. Distortions to the paper fibers and their network structure occur as a consequence of thermal deterioration [5, 10, 11]. Analysis of the changes to fibers and their woven structure have been limited to qualitative observations, and no research work has been conducted to quantify or measure changes to the insulation paper surface morphology occurring as a consequence of thermal aging.

The motivation for this research is for the development of an optical method to estimate deterioration in power transformer cellulose paper by using a combination of microscopy and image texture analysis. Optical methods are desirable for this application because they can provide a less invasive method for direct assessment of the insulation where sample sizes needed for analysis could be reduced from the established industry method; degree of polymerization test. Optical methods also have the potential for *in-situ* measurement in which the need to remove a sample may be eliminated entirely.

1.2 Research Objectives

The first objective of this research is to apply texture analysis methods to thermally aged transformer cellulose insulation to characterize how texture features change as a function of thermal deterioration level and to correlated this data with degree of polymerization measurements.

The second objective in this research is to examine how image texture analysis features

may be used with machine learning techniques for automated classification of thermally deteriorated transformer insulation. The purpose of this objective is to evaluate the potential of microscopy and image texture analysis as a method for the condition assessment of power transformer paper insulation.

1.3 Outcomes and Contributions

In this research, accelerated aging experiments were used successfully to produce a set of kraft paper samples belonging to four coarse deterioration levels roughly categorized as new-condition, aged, end-of-life, and beyond end-of-life condition. Two texture analysis methods have been applied to transformer winding insulation kraft paper to analyze microscopic surface morphological changes in the paper caused from thermal deterioration. One of the texture analysis methods is a traditional, statistical histogram based technique [12,13], while the second is a transform type method based on the two-dimensional Wavelet transform [14, 15].

A key outcome obtained in this research is finding that a number of statistical texture features appear well correlated with degree of polymerization (DP) measurements obtained from a set of thermally deteriorated kraft paper samples. Results have shown that a few statistical texture features share a logarithmic relationship with DP, and vary linearly with tensile strength. Another important outcome obtained in this research has been the implementation of statistical and Wavelet texture features in machine learning algorithms to train an automated classifiers that can estimate deterioration level into one of the four aging levels at high accuracy, with a classification error of 6% or less.

To the author's best knowledge, this Ph D. thesis is the first research work to attempt measurement of thermal deterioration changes in the transformer winding paper insulation by applying texture analysis to microscopic images of paper. The finding that certain statistical texture features trend proportionately to tensile strength of the transformer in-

sulation paper is a novel finding, and implies that the mechanical strength of the paper is directly related to the morphological changes which occur to paper fibers and their network structure in response to thermal deterioration.

1.3.1 Publications

A list of publications prepared or planned for preparation during the course of this research are listed below in chronological order:

- A journal publication describing results from statistical texture analysis on microscopic images of thermally deteriorated paper samples was published in [16]. This paper provides an analysis results obtained from automated classification of insulation paper belonging to one of four deterioration levels. The classifier is derived from the statistical texture analysis features after processing by standard machine learning techniques.

- A conference paper describing results from statistical texture analysis of microscopy measurements performed on transformer pressboard electrically deteriorated from surface partial discharges was published in [17]. However, results from these experiments were largely inconclusive, and as a result this work is considered to be outside the main scope of this thesis. Discussion and analysis from these experiments are detailed in Appendix B.

- A conference paper on the correlation between DP measurements from thermally deteriorated paper insulation samples and statistical texture analysis features from microscopic images of the thermally deteriorated paper samples was published in [18].

- A conference paper which presents a portion of results obtained from Wavelet texture analysis on thermally deteriorated paper sample has been submitted and accepted for conference presentation in [19].

- A final journal publication on the complete results obtained from Wavelet texture analysis along with comparison to the statistical based results is in preparation and planned for submission by February 2018.

1.4 Organization/Outline of Thesis

This thesis is organized in six chapters with content as described below:

Chapter 1: Presents an introduction to this research with motivation, research objectives, and main contributions and outcomes of the research.

Chapter 2: Presents background technical information applicable to this research work. Details on the power transformer insulation system construction are discussed along with deterioration mechanisms. Existing methodologies used for detection of insulation deterioration are reviewed along with discussion on morphological changes occurring in paper micro-structure as a consequence of thermal stress. An introduction to texture analysis is also presented with discussion on applications.

Chapter 3: Presents the experimental test arrangement for preparing thermally deteriorated paper samples and the microscopy measurement arrangement. Initial observations from microscopic images of thermally deteriorated paper are discussed. Results for degree of polymerization measurements on the prepared samples is presented.

Chapter 4: Presents results from texture analysis by a statistical based histogram method called the Spatial Grey Level Dependence Method (SGLDM). Texture features extracted from the SGLDM method are analyzed in terms of their variation and sensitivity to thermal deterioration and correlated with DP measurements. Machine learning techniques are applied on the SGLDM features to determine the effectiveness of this texture analysis method for automated estimation of deterioration.

Chapter 5: Presents results from a transform based texture analysis method which uses a two-dimensional Wavelet transform to extract texture features from thermally deteriorated paper sample microscopy images. Identical to the approach used for the SGLDM method in Chapter 4, the Wavelet texture features are evaluated in terms of their variation and sensitivity to thermal deterioration and a correlation with DP measurements is analyzed. Machine learning techniques are applied to the Wavelet features to determine the effectiveness of this texture analysis method for automated estimation of deterioration.

Chapter 6: The thesis is concluded by discussing the results obtained in relation to the original research objectives stated in Chapter 1. A discussion on future work that would improve and expand on this thesis work is presented.

Appendix A: Formulae used for machine learning methods; Linear Discriminant Analysis and Principal Component Analysis are presented.

Appendix B: Results and analysis from electrical stress by surface tracking partial discharge experiments on transformer pressboard insulation are presented.

Appendix C: A brief method description for the viscometric degree of polymerization test is provided as background.

Chapter 2

Background and Literature Review - Power Transformer Insulation System, Condition Assessment Methods, and Texture Analysis

In this chapter, a brief overview of power transformer construction and insulation systems design will be presented along with a description of the common deterioration processes and failure mechanisms. Morphological changes occuring in kraft paper as a consequence of thermal deterioration will are described along with a description of changes to the paper mechanical properties.

A review of existing transformer paper insulation condition assessment methods are covered along with discussion regarding their strengths and limitations. Finally the concept of texture analysis will be introduced with references to current applications in paper measurements.

2.1 Power Transformer Insulation Materials and Construction

The basic design of the power transformer has remained conceptually similar since the 1920s [20–22]. The tranformer core is made from steel laminations, stacked and compressed to form a closed magnetic circuit and the windings are made from copper or aluminum turns wound around the core. The core and windings are housed inside of a steel tank with the electrical insulation system.

The most common insulation materials in power transformers use a combination of electrical grade mineral oil and oil-impregnated paper. The insulating oil occupies a majority of the insulation volume. Most of the electrical strength in the power transformer insulation system is attributed to the fluid component [23] which also provides cooling to the core and coils of the transformer. Although refined mineral oils are the most common dielectric fluid used for insulation in power transformers, some alternative fluids such as synthetic or vegetable oils are used in special applications [1, 24].

The oil-impregnated paper materials are layered on or around the energized windings [23, 25]. The most common material used for the solid insulation component in power transformers is kraft paper. Kraft paper is an unbleached paper, brown in color, made from softwood coniferous trees such as spruce and pine [25]. Kraft may be manufactured as plain or thermally upgraded, where modifications during the pulping process improve the paper resilience to thermal degradation [26]. The paper is constituted with interwoven fibers which individually are approximately $50\mu m$ in diameter by $1mm$ in length [27].

The paper materials in power transformers serve a number of purposes. Firstly, the paper provides electrical separation of live parts, insulating between winding phases, winding turns, as well as between the windings to the core, or tank. Secondly, paper materials mitigate the propagation of partial discharges in the oil. Bare conductors in oil are far less

effective at mitigating ionization processes that produce partial discharges in oil [25]. In addition to electrical insulating benefits, paper materials also provide mechanical support to the windings, and guide the flow of insulating fluid as coolant to the core and windings.

Examples of these different forms of kraft cellulose papers and their use in a power transformer is shown in Fig. 2.1. The kraft paper tape constitutes the major portion of the transformer solid insulation. This paper tape is wrapped on the winding conductors to insulate individual turns from one another. To insulate the lead connections from the transformer winding to high voltage bushings, often a different type of kraft paper, called crêpe tape, is used. Crêpe tape is more elastic than the kraft paper tape and absorbs more oil per volume than regular kraft paper. For electrical insulation barriers between the high-voltage to low-voltage windings, between phases, and between the windings and the core or tank, a more dense cellulose product called pressboard is used. Pressboard is also used for bracing the space between the winding discs to allow for the flow of oil as coolant.

In this thesis, plain kraft winding insulation paper is analyzed in thermal deterioration experiments. Although pressboard and crêpe paper insulation degrade similarly to the winding insulation paper when under thermal stress, the winding insulation paper is more commonly associated with electrical insulation failures. The mechanism of winding insulation paper failure is discussed in Section 2.2.

2.1.1 Chemical Composition of Cellulose

The chemical composition of kraft paper contains approximately 95% cellulose. Cellulose is an organic polymer with a molecular structure as shown in Fig. 2.2. The structure shown in Fig. 2.2 depicts the cellulose monomer. This monomer is repeated in long chains to form polymer cellulose molecules and in new kraft paper, polymer molecule chains of with lengths of approximately 1000-1500 monomer units are present.

In kraft paper, intermolecular bonds are formed between adjacent cellulose molecules

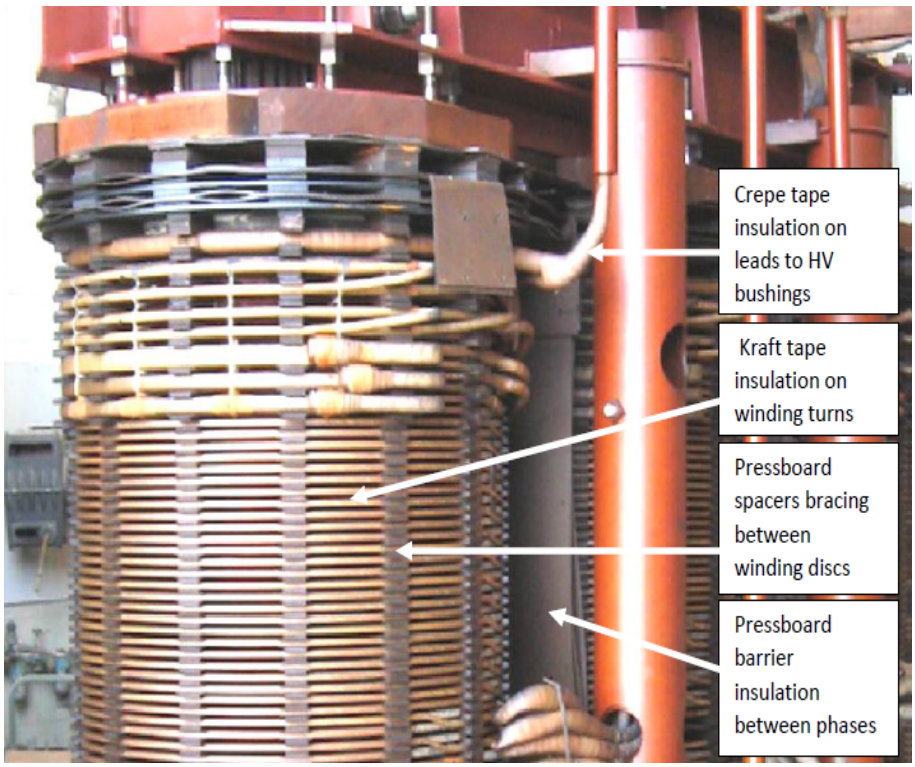

Fig. 2.1. Transformer core and coils removed from tank. Kraft tape winding insulation, crêpe tape HV bushing lead insulation, pressboard spacers between discs, and pressboard barriers between phases are identified by arrows.

in groups of approximately 2000 molecules. The groups make up fibrils that constitute cell walls of individual paper fibers [27]. In the finished kraft paper, the fibers are interwoven in a network. Characteristics of the fibers and their interwoven network determine many physical properties about the kraft paper which are important for their use in power transformers. For example the density of the paper network structure can affect its porosity for impregnation of insulating oil and its mechanical strength [23].

When kraft paper is subjected to thermal stress, breaks in the intermolecular bonds occur along with scissions breaking the chain cellulose molecules. When breaks in the polymer molecules occur, the molecule length is reduced and by reducing the length of cellulose molecules changes in the paper properties occur; the most significant of which affect the mechanical strength of the paper. In Section 2.2.2, the changes in paper properties progress, and their impact on transformer reliability will be discussed. The standard test for DP [9] in paper is an indirect method for estimating the average length of cellulose molecules in electrical insulation paper materials. The DP test will be described in Section 2.3.4. New kraft paper after processing and impregnation by mineral oil may be expected to have cellulose molecules of 1000 monomer units or greater, while transformer insulation which is considered to be deteriorated to an end-of-life condition, may be expected to have cellulose molecules with 200 monomer units or fewer on average.

2.2 Deterioration Mechanisms and Failure Modes of the Transformer Insulation System

2.2.1 Mineral Oil Deterioration

Although a majority of transformer failures are not caused by deterioration of its mineral oil. Indirectly, the degradation of oil will accelerate the deterioration of paper materials in the power transformers [28]. Deterioration of insulating oil is mainly caused by oxidation, which

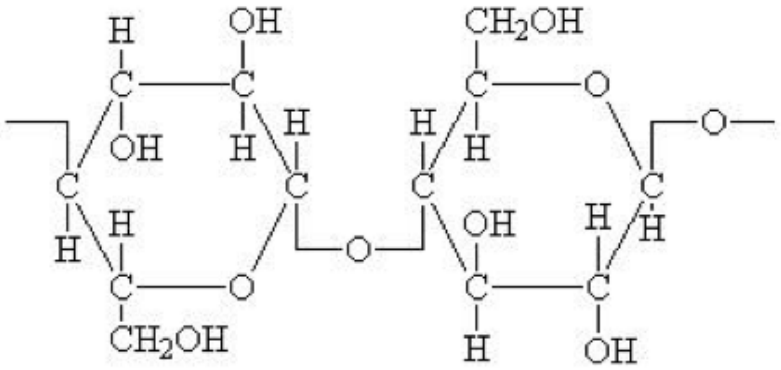

Fig. 2.2. Molecular structure of cellulose.

is a chemical process where ambient oxygen reacts with the transformer oil; using heat as a catalyst [1, 29]. When oxidation of the insulating oil occurs, it initiates chemical changes that produce dissolved acids and water in the oil as well as other other chemical byproducts that thicken the oil. Thickening of the oil impacts flow which therefore hinders cooling of the transformer core and windings [27]. These chemical byproducts can also produce low molecular weight acids and water in the oil that may accelerate deterioration of the paper. Moisture in the oil also reduces the oil's dielectric strength and enables the inception of partial discharges or internal arcing on paper surfaces inside the power transformer. These discharges can cause additional heating of paper materials and therefore accelerate the thermal deterioration of the paper [30]. In extreme cases, partial discharges themselves may lead directly to failures of the insulation system.

While the production of water and sludge in the insulating oil are undesirable, failures due to deteriorated oil in power transformers is uncommon. Utilities regularly maintain insulating oil by replacing or reprocessing the oil to remove sludge and moisture. Preventative measures may also be taken by adding inhibitor agents to the oil. These agents reduce acidification and the accumulation of sludge by reacting with the byproducts of oxidation, to make these byproducts readily soluble in oil [1].

2.2.2 Thermal Deterioration of Kraft Paper

The operational life of power transformers are mainly dependent on the condition of the paper insulation. The most common deterioration mechanism of the paper insulation component in power transformers is caused from thermal stress [26]. Over time, heat produced by the transformer core and windings during normal operation, thermally ages cellulose materials, resulting in a loss of their mechanical tensile strength. As this deterioration becomes significant, the cellulose materials become brittle [2, 6].

Many transformer failures occur when the deteriorated paper insulation is subjected to a system disturbance, such as a through-fault or load rejection [2]. Such electrical system events cause abrupt electromechanical forces on the windings which can disturb the brittle winding insulation between turns. In Fig. 2.1, the winding insulation paper is shown with kraft tape insulation on radially wound turns. These turns are wrapped tightly against one another. When the insulation becomes brittle from thermal deterioration, the likelihood of the paper tearing is increased when the tensile strength has been compromised due to thermal aging. Tearing leads to turn fault, which is a metal-to-metal contact between adjacent turns [2, 6]. The turn fault produces high circulating currents and a rapidly increasing temperature which in-turn leads to a thermal fault and insulation failure.

As mentioned in Section 2.1.1, the chemical mechanisms which lead to the paper becoming brittle relate directly to intermolecular bonds between cellulose molecules that constitute the paper, as well as the average length of the polymer cellulose molecules themselves [27]. Under thermal stress, the average length of cellulose molecules in the paper are reduced when thermal energy works to break bonds in the cellulose. When chemical bonds in the paper cellulose are broken, byproducts of these reactions produce water, carbon monoxide, acids, glucose, and organic compounds known as furans. These byproducts may reside in the paper or be suspended in the oil after formation.

Water and acid byproducts from thermal deterioration have an influence of accelerating

the paper degradation further as the water released can lead to hydrolysis of the paper where the paper reacts chemically with suspended water in the oil, causing a secondary mechanism for breakdown of cellulose [6]. Low molecular weight acids created from pyrolysis of the paper can also react with cellulose to degrade the paper [28]. Similar to the occurrence of oxidative degradation in mineral oil (Section 2.2.1), suspended oxygen in the oil can react directly with outer hydrogen atoms. When such a reaction occurs, it too causes breaks in the cellulose molecule.

2.3 Methods for Power Transformer Insulation Condition Assessment

2.3.1 Electrical Diagnostic Tests for Power Transformers

There exist a number of electrical diagnostic tests that are performed on power transformers during maintenance outages. The most standard of these electrical tests are the insulation resistance and dielectric loss factor measurements [31]. The insulation resistance measurement involves applying a low magnitude direct voltage and measuring the change in leakage current over time. If the insulation resistance remains low during test, this can be indicative of an insulation problem. Similarly the measurement of dielectric losses can be indicative of an insulation problem if the power factor losses of the insulation are high. In either case, problems may be attributed to contaminants or moisture in the oil or paper [32] making these methods generally ineffective at isolating problems with solely the insulating paper.

A modern diagnostic method called dielectric frequency response (DFR) analysis obtains dielectric loss measurements over a range of test supply frequencies [33]. The method is most accurate at estimating the amount of moisture present in paper insulation. Because degradation of the transformer paper insulation generates moisture in the paper, DFR can be indicative of paper deterioration level [34]. However, this method is still a bulk measure-

ment and not suitable for detecting acute defects in the paper insulation system.

2.3.2 Dissolved Gas Analysis

The most common method of insulation assessment performed on power transformers involves analyzing samples of oil removed from the transformer. One of the analysis methods is called dissolved gas analysis (DGA) [7,31]. In performing DGA, an oil sample is retrieved from valves accessible externally to the transformer tank, usually at ground level. These samples may be retrieved while the transformer is in operation. Determination of content of gases dissolved in the oil is achieved by technique called gas chromatography. Measurement of the relative concentrations of gases present in the oil are indicative of certain insulation problems related to high temperatures, partial discharges, and/or internal arcing. The specific methodology for analyzing the transformer oil for detection of insulation problems is called dissolved gas analysis (DGA) [3, 7, 35].

Degradation of the insulation paper from DGA is sometimes detected by comparing the relative concentrations of carbon monoxide to carbon dioxide present in the oil. When the relative concentration of carbon monoxide is equal to or exceeds carbon dioxide, this is usually indicative of thermal stressing to the paper insulation [6, 36].

The shortcomings of using oil samples to detect insulation problems in the paper are due to the limitations associated with the methods being indirect. The analysis performed on a sample taken from the large volume of transformer oil may make the method insensitive to the detection of acute defects in the paper insulation system. Accumulation of gases in the oil could be contributed from small defects distributed to multiple regions of the paper insulation system, or they may be caused from a singular defect which is quickly deteriorating toward failure. This lack of sensitivity is the main drawback for making assessments about the paper condition from DGA.

2.3.3 Detection of Chemical Compounds in Insulating Oil

There are a number of chemical markers that may be present in oil that are indicative of paper degradation [37–39]. The most commonly cited chemicals found in oil samples that are considered indicators of paper deterioration are called Furan compounds [40], and are carbon ringed molecules which are a byproduct of breakdown of the cellulose chain molecules from thermal deterioration. Furan compounds become dissolved in the oil and can be measured using high-performance liquid chromatography (HPLC) [38]. Other work [41] has shown that the presence of low molecular weigh acids in the oil are a more serious indicator that the transformer may be much closer to failure.

However, the shortcomings of finding chemical compounds suspended in the oil to detect paper degradation are identical to the shortcomings associated with DGA. Measurement of furanic compounds as a diagnostic tool for insulation paper are ineffective at discerning between distributed and acute defects in the transformer winding insulation.

2.3.4 Measurement of Degree of Polymerization

The most established and accurate method for direct assessment of thermal deterioration in the paper insulation component is the DP test [8, 9]. The DP test has been shown to correlate well with mechanical tensile strength of cellulose paper. The test is performed on a sample of paper taken from the transformer which is then dissolved in a special solution to form slurry. The viscosity of the slurry has been shown to be directly proportional to the average length of the cellulose molecules in the original sample of paper. As paper is thermally aged it forms breaks in the cellulose molecules to form shorter chains. This reduces the mechanical strength of the paper and reduces the DP. In general, for new transformer paper insulation DP is expected between 1000-1200 units. If the paper becomes critically aged and its tensile strength reduced so that it is a high risk for failure, DP is expected to be less than 200 units, at which point the tensile strength has reduced to less than 30% of

its original strength. [2, 6].

The relationship between paper tensile strength and degree of polymerization is well documented in numerous industry standards and guides [2, 6, 8, 9]. In Fig. 2.3, the graphs display this relationship. The upper graph shows experimental results obtained by Emsley *et al.* [42], and Lundgaard *et al.* [43] where tensile strength and DP were measured from thermally deteriorated kraft paper samples. The data from both measurement sets appears to show a logarithmic relationship between tensile strength and DP. The data set have been fitted by a natural log curve using least-squares curve fitting. Equations for these curves are displayed on the graph. The lower graph in Fig. 2.3 shows the relationship between tensile strength and the inverse of DP multiplied by a factor of 1000 ($1000/DP$). This relationship produces a straight line and is referenced in [42]. These relationships between tensile strength and DP will prove useful in the analysis of texture features later in Section 4.3.2.

Although the DP test is a direct measurement making it more suitable for detection of acute defects, its main drawback is that it requires a sample of paper removed from the power transformer. As mentioned in Section 1.1, the downside to methods requiring a physical sample are that they are inconvenient and may not be performed while the transformer is in operation. They are also potentially invasive to the insulation system. The standard DP test requires a physical sample of $3g$ removed from the transformer winding [8, 9]. Removal of this much paper from a single region of the transformer winding could be potentially damaging to the transformer making the DP test impractical.

2.4 Alternative Methods for Paper Condition Assessment

Given the limitations of established methods available for power transformer paper condition assessment discussed in Sections 2.3.2 to 2.3.4, research exploring alternative methods have been explored [32]. For an alternative method to be desirable, it must provide benefits over

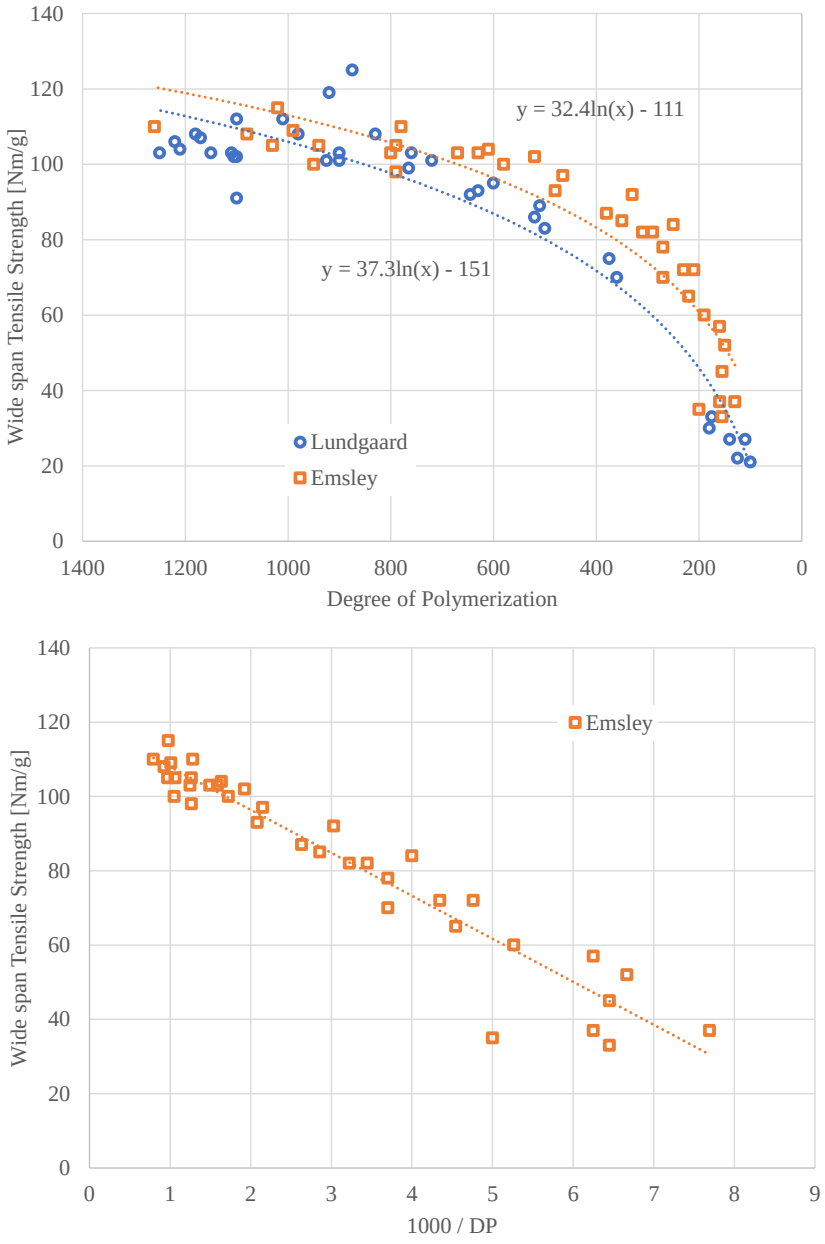

Fig. 2.3. Relationship between Tensile Strength and Degree of Polymerization from empirical data given in [42] and [43].

the established methods. Alternatives should be capable of direct assessment making them suitable to detect acute defects (unlike DGA and Furan analysis), while being less invasive than the DP measurement. Because the DP methods require relatively large sample size ($3\,g$)for analysis it is often considered too invasive. To be less invasive, alternative methods must reduce the required sample size or potentially eliminate the need for removal of a sample by allowing measurements be performed *in-situ*.

As already discussed in the previous section, the tensile strength of paper, is influenced by characteristics of individual fibers, their density, and their orientation inside the paper structure [23]. As paper thermally deteriorates it causes distortion to the paper fibers and their arrangement. This effect has been demonstrated using various microscopic imaging methods. In [5, 10, 44, 45] the authors used scanning electron microscopy (SEM) to show that thermal deterioration caused fissures and cracks on the fiber walls along with thinning of individual paper fibers and a loosening in the interwoven paper network.

Alternative to imaging methods which observe the surface morphological changes thermal aging, other research work has implemented methods which detect chemical changes in kraft paper. In [11, 46], Atomic Force Microscopy (AFM) was used to analyze thermally deteriorated kraft pressboard samples with results suggesting the reduction of certain molecular bonds was indicative of a deterioration.

Methods implementing infrared spectroscopy have been used with limited success in [47–50] to show that changes in molecular bond vibrations excited from spectroscopy were correlated with DP to allow for direct estimation of deterioration level. It is also noteworthy that the infrared spectroscopy methods in [50] demonstrated the possibility for *in-situ* measurements where a scanning probe was developed that could perform assessment of kraft paper without requiring removal of a sample. The infrared spectroscopy method promised the potential for significant advantage over the SEM and AFM methods in [5, 44]. *In-situ* measurement could be possible and direct assessment of the paper condition could be made

from data correlated to DP measurements. The SEM and AFM research work has been limited to qualitative observations of the changes without enabling direct estimation of deterioration level. Some limitations in accuracy were however observed for the infrared method in [50] when it was discovered that results could be affected by irregular reflectance due to variations of curvature on insulation surfaces and the enhanced scattering of paper in the optical to the near-infrared range.

In work conducted by the same research group involved in this thesis, optical speckle diffraction patterns were measured from the surface of kraft paper samples having varying levels of thermal aging [51]. This work demonstrated an ability to differentiate between different levels of thermal deterioration based on statistical texture analysis of the optical speckle diffraction pattern images.

In this research, optical microscopy is used for paper measurements on thermally deteriorated kraft paper samples. Compared with SEM and AFM, optical microscopy is a much more simplistic imaging approach. The paper and pulp industry have a lengthy history for using optical microscopy as a tool for quality assurance where paper samples are retrieved at different stages of production for microscopic analysis [52]. Microscopy measurements can be used to analyze individual paper fibers and their network structure.

One of the challenges concerning optical microscopy measurements on paper materials is that at high magnification, the varying surface profile of the paper network structure makes imaging difficult and can result in images with out-of-focus regions due to shallow depth-of-field of the optical measuring equipment [23]. Imaging of paper materials at lower magnification is more appropriate [23].

In Section 3.3 we will observe that at lower magnifications differences in bulk texture as a consequence of thermal aging are still observable using standard microscopy, and in Chapters 4 and 5 we will determine that these differences are measurable using texture analysis methods.

2.5 Texture Analysis of Images

2.5.1 Methods for Image Texture Analysis

Texture refers to the concept of perceiving physical attributes of a material surface. Surfaces may be perceived as rough, smooth, heterogeneous, or homogeneous. In computer vision and image processing, texture analysis refers to a class of mathematical procedures and models that are used to quantitatively characterize the spatial variations in images [13, 53–55]. These quantitative measures may or may not be associated with actual perception of texture. Methods for texture analysis, typically fall into one four categories: statistical, structural, model-based, and transform based methods [53].

Statistical methods are the most well-known and involve translation of an image into matrix or histogram representations of an image that contains information about the statistical frequency and/or variation of pixel intensities [12]. The most widely used method first presented by Haralick *et al* in [12] will be applied to thermally deteriorated kraft paper samples in Chapter 4.

Structure-based methods associate texture features with well defined structural elements or simple geometric shapes or contours. The analysis is defined in terms of placement of the structure at different locations of the image [53]. An example of a structure-based method may be to correlate a texture image with parallel spaced lines. If for example the image texture being analyzed had a checker board type pattern then depending on orientation we might expect the correlation to yield a large number. Conversely if the image texture appeared as small randomly distributed dots, then we would expect the correlation with parallel spaced lines to produce a small number. Structure-based methods are best applied to textures having very regular and predictable patterns. Structure-based methods were not applied to the microscopic images of thermally deteriorated paper. It will be shown in Chapter 3 that the paper surface texture is very random in nature, therefore making it

a poor candidate for texture analysis using structure-based methods.

In model-based texture analysis methods, an empirical model is developed for each pixel in an image by analyzing content in the surrounding pixels. These models are then used as feature descriptors [53]. In these methods the parameters of the model are estimated from a set of training images. Then the estimated parameters are used to quantitatively describe the entire image set being analyzed. These methods are useful in image segmentation where small areas of an image have distinctly different texture qualities than those modeled from regions covering the majority of an image. In thermal aging experiments performed in this thesis, we expect that the images of thermally deteriorated paper samples will have defects uniformly distributed in image frame, therefore model-based methods and segmentation have not been applied in this thesis.

Transform based texture analysis convert images into a new form while extracting textural information from the transformed images. Wavelet texture analysis is the most popular form of transform based texture analysis [56]. In Chapter 5 a method of Wavelet texture analysis will be applied to thermally aged kraft paper.

In instances texture analysis is used for discerning between material having different surface textures, features extracted from the texture analysis method are commonly processed using machine learning algorithms to enable automated classification of a material category, quality, or condition [57].

2.5.2 Industrial Applications for Image Texture Analysis

Statistical texture analysis on microscopic images of materials are used in a number of different industry applications ranging from analysis of wood materials, to quality assurance in the manufacturing of textiles [57,58]. For applications in the electrical apparatus industry, texture analysis has been used to qualify thin polyamide films for their suitability to install in electrical components [59].

A few publications have demonstrated the successful application of texture analysis on microscopic images of paper materials specifically [60, 61]. Similar to other industrial applications the motivation for work in this area is for improving quality assurance in the paper making industry. Given that the application of statistical texture analysis has been successfully applied for analysis of paper materials in other research work, this suggests that the proposed methodology to analyze changes in kraft paper surface morphology using texture analysis methods in Chapters 4 and 5 is reasonable.

2.6 Chapter Summary

The power transformer electrical insulation system is commonly composed of mineral oil and oil-impregnated kraft paper materials. Insulation failure can occur due to deterioration of the paper component when the paper is subjected to thermal stress. The common cause of insulation failure is due to the loss of mechanical tensile strength in the paper, which is attributed to a chemical changes occurring in the paper as a consequence of thermal deterioration. Kraft paper which is composed of 95% cellulose, loses tensile strength when the average length of cellulose molecules are reduced. Chemical reactions in the paper are activated by heat causing breakdown in the cellulose molecules. Coincident with changes in the mechanical properties of kraft paper, changes also occur to the microscopic surface morphology of paper as a consequence of thermal deterioration. These changes are perceptible using microscopic imaging methods such as SEM. With breakdown, paper fibers are distorted as cracks and fissures form on paper fibers.

Current methods for assessment of the paper insulation in power transformers have a number of limitations. Electrical diagnostic test methods such as insulation resistance, dielectric loss measurement, or dielectric frequency response analysis, are ineffective at isolating deterioration occurring in the paper component versus the oil insulation. Methods which involve analysis of an oil sample taken from the transformer are ineffective at detecting

deterioration of acute or regional insulation defects. Lastly, methods such as the DP or tensile strength tests require too large a paper sample retrieved from the transformer making the test too invasive and therefore impractical.

A brief overview of texture analysis in images and its methodologies have been presented. Given the nature of changes to the surface morphology of paper that occur from thermal deterioration, kraft paper appears to be a good candidate for texture analysis methods with intent to develop an alternative assessment method for the kraft paper materials in power transformer insulation.

Chapter 3

Experimental Method for Preparation of Thermally Aged Paper Samples and Microscopy Measurements

This chapter will cover experimental test arrangements used for preparing thermally deteriorated kraft paper from winding insulation samples for microscopic texture analysis. The experiments are designed to emulate deterioration mechanisms caused by in-service stresses present in the power transformer but in an accelerated manner. The results from DP measurements obtained on control samples are also presented for correlation to the statistical texture analysis results that will be discussed in Chapters 4 and 5.

Fig. 3.1. Turn insulation paper installed on a sample of winding conductor.

3.1 Description of Specimen Materials

The kraft paper used in thermal aging experiments of this research is a flat untreated cellulose based paper manufactured by Weidmann Electrical Technology Inc. The winding insulation paper samples were new/unused and not previously impregnated by insulating oil. The paper dimensions are 1.9 cm wide and approximately 76 μm (3 mil) thick as supplied. An example of turn insulation paper installed on a section of transformer conductor is shown in Fig. 3.1.

For thermal deterioration experiments, papers samples are impregnated by Luminol type TR mineral oil. Luminol TR is a transparent mineral oil, that is slight yellowish color. The oil was tested prior immersion of the cellulose papers to verify that the moisture content in the oil was less than 30 ppm water content by mass. As mentioned in section 2.2.2 high moisture content will accelerate the deterioration of the paper making it difficult to control the desired rate of deterioration in the experiment.

3.2 Preparation of Thermally Deteriorated Winding Insulation

The method for preparing thermally deteriorated winding insulation samples emulates an accelerated aging test method described in an industry guide used for thermal evaluation of combined liquid and solid electrical insulation components [62]. The use of accelerated aging under thermal stress is a common technique used in the evaluation of insulation material performance and compatibility between materials [63]. Although there is no specific standardized test method to explore the degradation of kraft paper materials used in power transformers, a number of different accelerated aging test arrangements have been reported [64]. Similar accelerated aging tests on oil-impregnated Kraft papers have been performed in other work focused on measuring the retained tensile strength after thermal stress at temperatures elevated above normal operating thermals of a power transformer [10, 65].

Samples of the kraft paper tape were cut individually to 3-4 cm in length. Two samples are prepared for each aging class; making eight samples in total. The approximate weight of each sample was 0.05 g. The samples were then inserted in cylindrical glass vials as shown in Fig. 3.2 and placed uncovered in an oven at $105°C$ for 24 hours to remove the preexisting moisture present in the paper caused from the ambient humidity [66]. This drying phase is required to obtain better control of the rate of paper deterioration in experiments; as discussed in Section 2.2.2 moisture has significant influence on the rate of paper deterioration due to hydrolysis chemical processes in the paper.

After drying, the samples were removed from the oven and immediately sealed, and weighed. The sample's weights after drying indicating that on average approximately 8% moisture by mass has been removed from the paper samples during the drying phase. Approximately $25mL$ of Luminol insulating oil was added to each vial to impregnate the paper samples as shown in Fig. 3.3.

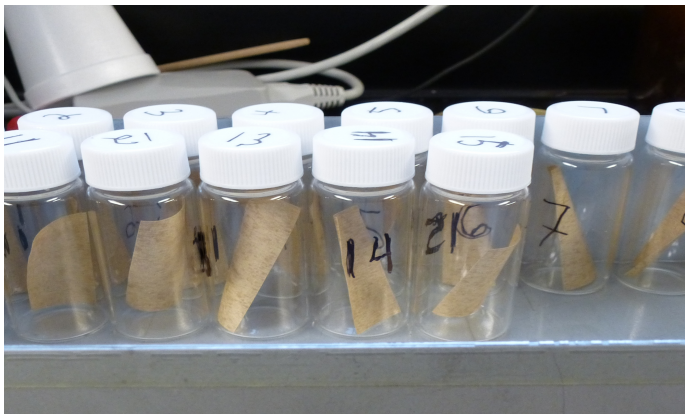

Fig. 3.2. Preparation of sample vials containing Kraft winding insulation for removal of pre-existing moisture. Samples dried for 24-hours at $100°C$.

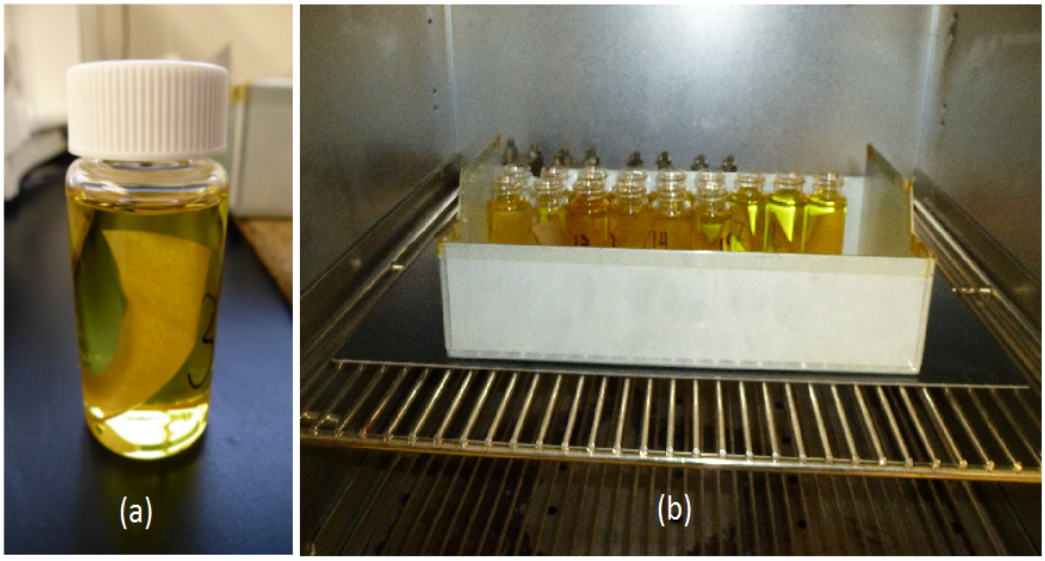

Fig. 3.3. (a) Sample vial containing winding paper insulation and $25ml$ of insulating oil, (b) Preparation of sample set for accelerated aging in an oven at 140°C

.

One set of vials containing oil-impregnated paper samples were sealed and stored in an air-tight box. These vials are intended to serve as new-condition transformer winding insulation after drying and impregnation. The remaining vials containing oil-impregnated paper samples were then returned to the oven at a temperature of 140°C for accelerated aging. Individual samples were removed from the oven after 120, 250, and 400 hour durations of accelerated aging. In each instance, the samples were sealed upon removal, and stored until microscopy measurements were made.

The accelerated aging temperature of 140°C was selected because it is sufficiently well above operating temperatures that the insulation would be exposed to during service. The same temperature was selected for aging experiments performed in [42, 44]. Industry standards [67] require that the maximum hot-spot temperature of a power transformer to be less than 80°C above the ambient temperature. Therefore assuming an ambient temperature of 35°C, the transformer winding paper insulation may be expected to reach as high as 115°C during normal operation. The accelerated aging temperature of 140°C used in these experiments is approximately 20% hotter than would occur in service. The aging durations of 0, 120, 250, and 400-hours aging duration were chosen based on the results obtained in [42] so as to achieve a suitable spectrum of aging conditions from new condition to end-of-life that could be analyzed using microscopy and texture analysis.

At the end of accelerated aging tests, the insulating oil color in the sample vials has become darkened from the thermal stress duration as shown in Fig. 3.4. The mineral oil color prior to thermal aging was a translucent, light yellow color as shown in Fig. 3.3. After 120-hours at 140°C the color is darkened to a translucent brown color, and after 250 and 400-hours the color became a dark opaque brown. This darkening is caused from the oxidation of the mineral oil as was described in Section 2.2.1. In section 3.3, we will see that this darkening has some influence on the microscopy images of paper samples.

Fig. 3.4. Sample vials containing paper samples and mineral oil after accelerated aging tests. From left to right in groups of 5, the vials contain samples aged 120-hours (first group), 250-hours (second group), and 400-hours (third group).

3.3 Microscopy of Thermally Deteriorated Paper Samples

After accelerated aging, paper samples were removed from the vials and cut into smaller sections approximately $1cm \times 1cm$. The sections were placed on microscope slides with a few drops of insulating oil taken from their respective vials and covered with glass cover slips to minimize exposure to air humidity. An inverted Olympus IX73 optical microscope was used to capture images of the samples at $10\times$ magnification in 256-bit grey scale. Care was taken to ensure that all images were captured with the same aperture and exposure settings. Between 50 and 65 sample images were captured for each of the four aging groups; new condition, 120, 250, and 400-hours of accelerated thermal aging at 140°C.

For statistical texture analysis, it was decided that $10\times$ magnification images was suitable because it provided a large enough area of the paper within the image field of view to provide a representative sample of the overall surface texture needed in texture analysis. At higher magnifications the texture images were not usable. Due to the shallow depth of field at higher microscope magnifications, some regions of the sample images were out-of-focus. Having out-of-focus regions in the images would produce errors in the texture analysis.

In Fig. 3.5, the influence of oxidized oil in the sample vials is obvious. The thermally deteriorated paper samples are stained by the oxidized oil causing the samples with more thermal deterioration to appear darker. This darkening is easily visible in microscopy measurements also. In Fig. 3.6, microscopy measurements from samples having new condition after impregnation, and 120, 250, and 400-hours of accelerated aging at 140°C are shown. The sample aged 400 hours is evidently darker in color than the new-condition sample. This darkening caused from staining by oxidized oil is not representative of what would occur in an actual power transformer where the large volume of the oil and its circulation during normal operation prevents the oil from reaching this level of oxidation. In Chapter 4, Section 4.1 image preprocessing methods that reduce the influence of sample darkening will be presented.

Changes to the paper surface morphology, as a consequence of thermal aging, are already evident in the microscopy images in Fig. 3.6. In the new-condition sample we can see pristine individual fibers in an interwoven network. As thermal deterioration progresses, after 120-hours we can see that the fiber walls that were once pristine, start to develop holes and fissures. After 250-hours we can see that although individual fibers are visible, there is a thinning of the fiber widths, and a higher density of cracks and fissures in the fiber walls. Finally, after 400-hours of thermal aging the breakdown of the fibers has progressed to the level that few individual fibers are visually perceptible. The high density of cracks and fissures makes for a more homogeneous appearing texture.

3.4 Degree of Polymerization Measurement

For correlation with results from statistical texture analysis of thermally aged paper samples, DP measurements were made on a set of control samples. These control samples were prepared in the same manner as described in section 3.2 only they have been prepared with $3\,g$ of paper immersed in mineral oil. This is the amount of paper recommended for DP

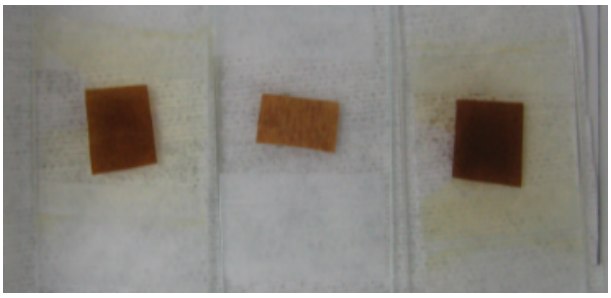

Fig. 3.5. Slides prepared for microscopy of thermally aged insulation paper. Notice darkening of paper from staining by oxidized oil. The sample on the left is aged 250-hours in insulating oil, the middle is aged 250-hours without oil, and the right is aged 400-hours in oil.

measurements in industry standards [9]. Two samples for DP measurement are prepared for each aging level. A short description of the viscometric degree of polymerization test method is provided in Appendix C.

The results from DP measurements are summarized in Table 3.1. Values for DP are an average of two independent measurements obtained on the two separately prepared reference samples. The DP values shows that a good spectrum of paper condition has been obtained for analysis. The new-condition sample is 717 DP units with nearly full remaining life estimated. The small reduction in DP for the new-condition paper was likely caused from the drying phase performed at 100°C which was effective at reducing the moisture content to 3.15%. With this level of moisture after drying, we can assume that degradation due to moisture was well-controlled in these experiments. The sample aged 120-hours resulted in a DP of 316, which corresponds to an estimated remaining life of 34%, which is a significantly aged sample. The sample aged 250-hours produces a sample with a DP of 193, which just surpasses the conventional end of life criteria of 200. Finally, the sample aged 400-hours corresponds to a DP of 115, which is well-beyond the end of life criteria.

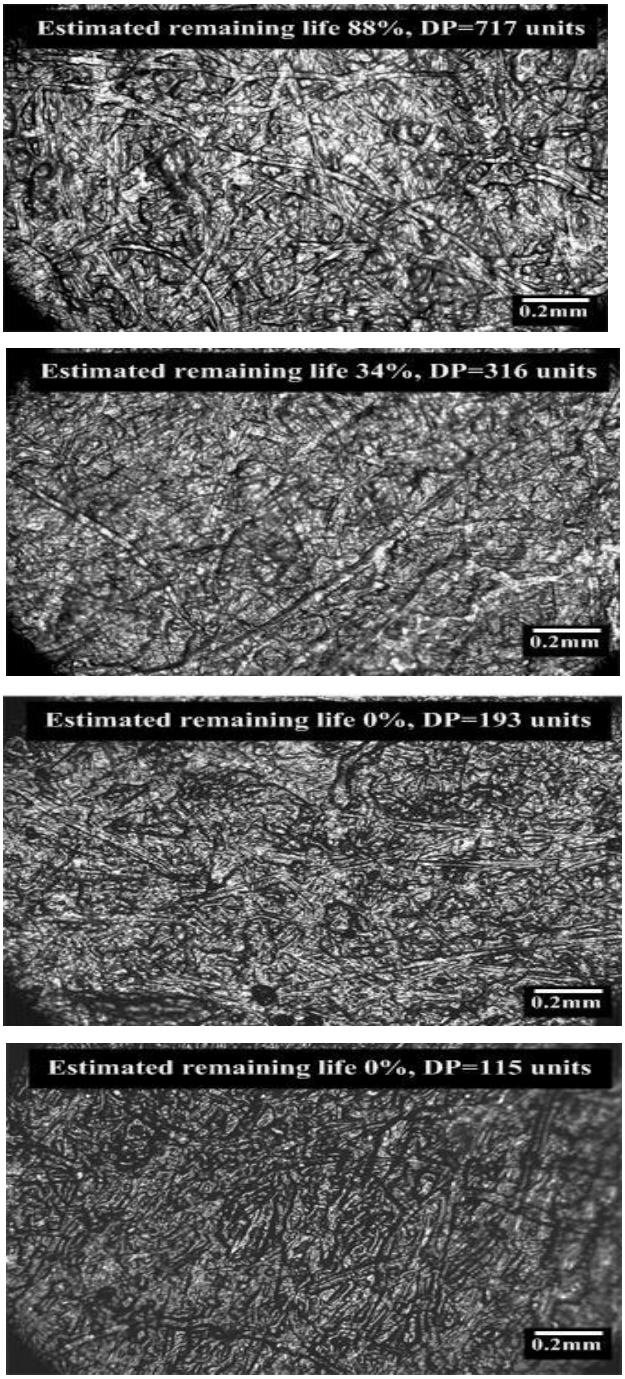

Fig. 3.6. Microscopy images of winding insulation Kraft paper deteriorated for 0, 120, 250, and 400 hours at $140°C$; corresponding DP values of 717, 316, 193, and 115 DP units.

Table 3.1. Degree of Polymerization measurements on samples aged 0, 120, 250, and 400 hours at 140°C.

Thermal Aging Duration at 140ºC	Degree of Polymerization	Estimated Remaining Life	Moisture Content
0-hours	717	88%	3.15%
120-hours	316	34%	-
250-hours	193	0%	-
400-hours	115	0%	-

3.5 Chapter Summary

In this chapter, an experimental method for the preparation of thermally aged kraft paper samples is described. The experimental method appears to have been effective at obtaining a set of paper samples with a good distribution of aging levels from nearly full remaining life, to well past end-of-life criteria in terms of the sample DP measured values. Microscopy images of the paper samples show clear textural changes as a consequence of thermal deterioration. New condition paper contains fibers that have pristine fiber walls. With progressive thermal aging, cracks and fissures develop in the fiber walls until the surface morphology of the paper becomes more homogeneous in appearance due to the density deterioration. A byproduct of the thermal aging experimental method, is the darkening of the paper samples caused from oxidation of the insulating oil. The oxidized mineral oil stains the paper samples creating an artificial level of darkening that is not representative of what would occur in an actual power transformer.

Chapter 4

Statistical Texture Analysis of Thermally Deteriorated Paper Samples by Spatial Grey Level Dependence Method

In this chapter, the microscopic images of thermally deteriorated paper samples are analyzed using a statistical-based texture analysis method called the spatial grey level dependence method (SGLDM). This method is also commonly referred to as the grey-level co-occurrence method (GLCM). The results and analysis of the computed statistical texture features is presented along with automated classification of deterioration level of using standard machine learning techniques.

4.1 Preprocessing of Thermally Deteriorated Paper Sample Microscopic Images

Image processing is the manipulation of a digital image to produce an output image with modified or enhanced properties as compared to the original in order to achieve a specific objective [68]. Prior to performing statistical texture analysis on the images of deteriorated paper samples, image preprocessing is required in order to convert the microscopic images from color to an 8-bit grey-scale image format, and to normalize differences in tone or brightness between paper sample images. Some tonal or brightness differences are due to inconsistent illumination, but more significantly, in the case of thermally deteriorated paper samples, differences are due to staining of the paper samples caused by oxidation of the insulating oil. In Chapter 3, it was shown that after 250-hours or 400-hours of thermal stress the samples become significantly darkened by staining from the oxidized mineral oil. Similar observations of discoloration due to thermal stress experiments has been observed in [10,21,45]. These variations are problematic for statistical texture analysis which requires comparison of sample images with varying levels of deterioration. Brightness or color changes may mistakenly be interpreted as textural changes. Because this darkening is not representative of what could realistically occur in a power transformer while in-service, preprocessing is used to normalize out differences in tone and darkness so that only the textural differences will be analyzed.

4.1.1 Image Preprocessing Grey-Scale Conversion

In grey-scale images, all color information is removed and only the intensity information about individual pixels is retained. In an 8-bit grey-scale image there are 256 discrete shades of grey ranging between 0-255, where 0 represents the darkest pixel grey-value (black) and 255 the brightest pixel grey-value (white).

The pixels in the original color image are defined by an RGB color model. To convert a color to an equivalent grey-scale intensity the red, green, and blue value coefficients are scaled by:

$$I_{rgb2gray} = (0.2989 \times R) + (0.5870 \times G) + (0.1140 \times B), \tag{4.1}$$

where R, G, and B are the respective red, green, and blue color values and $I_{rgb2gray}$ is the equivalent greyscale intensity level rounded to the nearest integer value. The formula in (4.1) is adopted from the commercial software package in [69].

4.1.2 Image Preprocessing Normalization

As discussed in Section 3.2 the darkening of thermally deteriorated paper samples was caused by insulating oil which had oxidized in the sample vials during the accelerated aging. The accelerated aging temperature of 140°C used in this experiment produced more rapid oxidation of the oil than would occur during normal transformer operating temperatures. As a consequence, field-aged paper samples would not be as dark as those subjected to accelerated ageing in this experiment. The darkening of the paper samples shows up prevalently in microscopy measurements as discussed in Section 3.3. The relative change in sample darkening is evident by the general shift of grey scale pixel intensities towards lower values and the average pixel intensity levels became 4.7%, 35.5%, and 47.4% darker after 120, 250, and 400 hours of thermal degradation at 140°C. Because the texture analysis methods extract information from the spatial arrangement of pixel intensity values in an image, the sample darkening can have an influence on the computation of texture features.

To address the problems of tonal variations and artificial darkening due to staining by oxidized oil, normalization methods are employed in preprocessing. Two different methods of image normalization enhancements are utilized in this research; minimum-maximum normalization, and histogram equalization. Min-max normalization increases image contrast

by linearly extending the range of intensities over the full range between 0-255 [68]. Each pixel is scaled using:

$$I_N = (I - I_{\text{Min}}) \cdot \frac{(I_{N\text{max}} - I_{N\text{min}})}{(I_{\text{Max}} - I_{\text{Min}})} + I_{N\text{min}} \tag{4.2}$$

where I represents any pixel within the original image, and I_{Min} and I_{Max} are the respective minimum and maximum pixel intensities within the original image. The values $I_{N\text{min}}$ and $I_{N\text{max}}$ are the minimum and maximum pixel intensities for the full range; 0-255. Each pixel in the original image is transformed by this equation and the final normalized pixel values in the normalized image are represented by I_N.

Although minimum-maximum normalization enhances contrast and reduces a portion of variation in brightness between sample images, differences in color between sample images will still be present after normalization. Histogram equalization permits normalization of sample images by evenly distributing the pixel intensity level content over the full range.

The algorithm for histogram equalization is adopted from [68] and given in (4.3) and (4.4). Equation (4.3) computes the relative probability p_r that a grey-level r_k occurs in an input image that has $(L-1)$ different grey-level intensities. The parameter n represents the total number of pixels in the image, and n_k the number of instances that pixel intensity k occurs in the image.

$$p_r(r_k) = \frac{n_k}{n} \qquad \text{where k = 0, 1, 2,...., (L-1)} \tag{4.3}$$

The transformed output image is represented by s_k, given in (4.4). The transformation, $T(r_k)$, effectively transforms each pixel grey-level such that it is scaled relative to its frequency of occurrence in the original image r_k and its corresponding cumulative distribution function value. In other words each pixel intensity value is re-mapped to its cumulative density value rescaled in the pixel intensity range between 0-255.

$$s_k = T(r_k) = floor((L-1)\sum_{j=0}^{k} p_r(r_j)) \qquad \text{where k = 0, 1, 2,..., L-1} \tag{4.4}$$

The effect of these normalization methods on the images of a thermally deteriorated kraft paper samples is shown in Fig. 4.1. The far left column of Fig. 4.1 shows images of samples aged 0, 120, 250, and 400 hours at 140°C. These are images after grey-scale conversion but prior to normalization. Images in the center and right column of Fig. 4.1 show sample images have been preprocessed by minimum-maximum and histogram equalization normalization respectively. For the minimum-maximum normalized images we can see that there is a slight improvement in contrast for the very dark thermally aged sample at 400-hours of thermal stress. However, the general trend towards darkening of the sample images as a function of aging is still present, and there is only a modest improvement from the original unprocessed images.

For the images normalized by the histogram equalization method, the influence of the darkening color shift has been compensated for by normalizing the average grey level to the median in the range between 0-255 and uniformly distributing the grey-scale level intensities over the range. In doing so contrast has been enhanced and textural details are more visible.

4.2 Spatial Grey Level Dependence Method (SGLDM) Transform

The spatial grey level dependence method (SGLDM) converts grey-scale images into a histogram matrix containing information about frequency of occurrence of each pixel grey-level intensity value between 0-255, along with information about their arrangement spatially within an image [12]. The SGLDM histogram matrix is a square matrix with the number of rows and columns equivalent to the number of grey levels in the original sample image. The matrix is populated by recording the number of instances in an image that a pixel

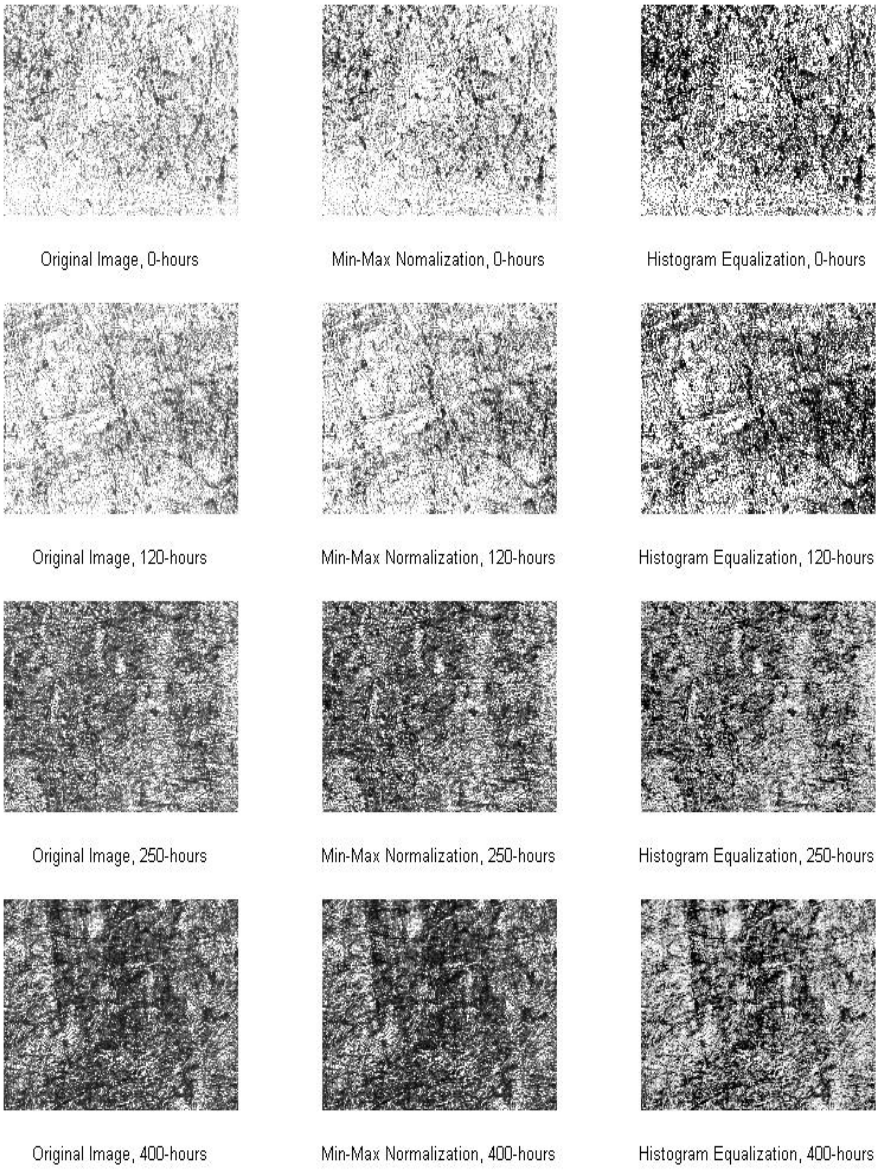

Fig. 4.1. Original images of thermally deteriorated transformer winding paper compared to minimum-maximum and histogram equalization normalized images at 0, 120, 250, and 400 hours of thermal stress at 140°C.

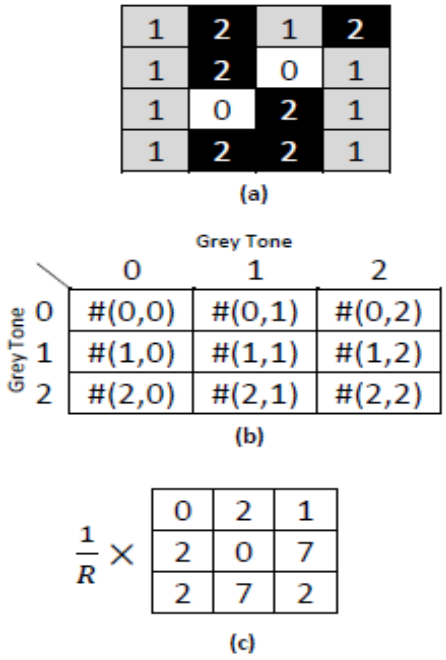

Fig. 4.2. Example computation for SGLDM matrix on an imaginary 4×4 sample image. The parameter R in (c) represents the sum of all elements in the matrix.

having a certain grey level intensity appears next to another pixel having a certain grey level intensity. An example for the computation of an SGLDM having three grey levels is provided in Fig. 4.2. In this example, an original image is represented by the matrix shown in Fig. 4.2a which has colored cells with varying grey-level intensity values of 0, 1, and 2. The grey-tone map in Fig. 4.2b illustrates how the SGLDM is populated. If the SGLDM is used to display the number of times a specific grey-level is neighbored by another specific grey-level at directions of 0° and 180° then the result is as shown in Fig. 4.2c. For example, the number of times the grey-level 2 is neighbored by the grey-level 1 is equal to seven. This corresponds to the grey-tone row 2 and column 1 shown in Fig. 4.2c. Finally, the SGLDM is normalized by the sum of all grey level intensities present in the original image.

In this work, the insulation paper sample images were captured with 256 grey scale levels, therefore the size of the SGLDM matrices are 256×256. Statistical textural features

of the original sample images were computed by performing mathematical operations on the SGLDM. Eleven textural features in two directions within the plane of an image are extracted. One direction for horizontal neighboring pixels (0° and 180°) and the other for vertical neighboring pixels (90° and 270°). Each microscopic image of deteriorated paper is converted in to a feature vector containing 22 texture features in total. Formulas for the texture features is provided in Section 4.2.1 along with a qualitative description of the feature meaning.

4.2.1 Haralick Statistical Texture Features

The formulas for statistical texture features are shown in (4.5)-(4.17) below and have been adopted from [12]. The cell entries of the SGLDM matrix are represented by $p_{(d,\theta)}(i,j)$ where d and θ represent the distance and angle relative to a reference pixel used in constructing the SGLDM. The i^{th} row and j^{th} column of the SGLDM matrix are identified by (i,j). As was mentioned in Section 4.2, the SGLDM matrix has been defined using a distance $d = 1$ pixels from the reference pixel and at angles 0° and 180° for one complete feature set. Another set has been defined using the vertical neighboring pixels at 90° and 270° from the reference pixel. In total twenty-two features are computed for each image.

Angular Second Moment: In (4.5), the feature angular second moment (ASM) may be described as a measure of uniformity in the pixel grey-scale intensities contained in the original image. For an image having a large number of pixels with similar grey-scale intensities, it will result in a large ASM feature quantity.

$$\textit{Angular Second Moment:} \quad F_1 = \sum_{i=1}^{N}\sum_{j=1}^{N} p^2_{(d,\theta)}(i,j) \tag{4.5}$$

Contrast: The feature described by (4.6) is a measure of contrast in the original image. For an image containing a high number of bright pixels neighbored by dark intensity pixels,

the contrast feature quantity will be high.

$$\textit{Contrast Feature:} \qquad F_2 = \sum_{n=1}^{N} n^2 \Bigg\{ \sum_{i=1}^{N} \sum_{j=1}^{N} p_{(d,\theta)}(i,j) \Bigg\}, \quad Where \quad n = |i-j| \tag{4.6}$$

Variance: A statistical measure of the overall variation of pixel intensities in the original image. The paramter μ represents the global mean of the SGLDM histogram matrix. Images containing a large variation of pixel intensities will have high variance feature quantity.

$$\textit{Variance (Sum of Squares):} \qquad F_3 = \sum_{i=1}^{N} \sum_{j=1}^{N} (i-\mu)^2 p_{(d,\theta)}(i,j) \tag{4.7}$$

Inverse Difference Moment (IDM): Inverse difference moment (4.8) is a measure of the local homogeneity in an image. Images containing pixels neighbored by other pixels with same or similar intensity will results in large inverse difference moment feature quantity.

$$\textit{Inverse Difference Moment (IDM):} \quad F_4 = \sum_{i=1}^{N} \sum_{j=1}^{N} \frac{1}{1+(i-j)^2} p_{(d,\theta)}(i,j) \tag{4.8}$$

Sum Vector: A sum vector expressed in (4.9), is obtained from the SGLDM histogram matrix. The sum vector is computed from the addition of the histogram matrix cell entries where the cell indices satisfy the condition that $k = i + j$ in the range from 2 to $2N$. The sum vector is used in the computation of features F5, F6, and F7 given by (4.10) to (4.12).

$$p_{(x+y)}(k) = \sum_{i=1}^{N} \sum_{j=1}^{N} p_{(d,\theta)}(i,j), \quad where \quad k = i + j \tag{4.9}$$

Sum Average: The sum average feature in (4.10) computes the average value of the sum vector in (4.9).

$$\textit{Sum Average}: \qquad F_5 = \sum_{i=2}^{2N} i \cdot p_{(x+y)}(i) \tag{4.10}$$

Sum Variance: Expressed in (4.11), sum variance computes the variance of entries in the sum vector in (4.9) about the sum average F5 from (4.10).

$$\textit{Sum Variance} \qquad F_6 = \sum_{i=2}^{2N} (i - F_5)^2 \cdot p_{(x+y)}(i) \tag{4.11}$$

Sum Entropy: Equation (4.12) computes the entropy of entries in the sum vector in 4.9. Entropy is commonly described as a measure of disorderliness.

$$\textit{Sum Entropy:} \qquad F_7 = -\sum_{i=2}^{2N} p_{(x+y)}(i) log(p_{(x+y)}(i)) \tag{4.12}$$

Entropy: Equation (4.13) calculates the entropy of the original image, which is a measure of chaos or disorder in an image. The statistical texture feature for entropy is related to the information theory definition of entropy which relates to the density of information in an image [71]. Entropy is inversely related to inverse difference moment in 4.5 where a completely homogeneous image would have little information and thus low entropy. Conversely an image having densely concentrated details would yield a large entropy quantity.

$$\textit{Entropy:} \qquad F_8 = -\sum_{i=1}^{N} \sum_{j=1}^{N} p_{(d,\theta)}(i,j) log[p_{(d,\theta)}(i,j)] \tag{4.13}$$

Difference Vector: Equation (4.14) calculates a difference vector from the entries of the SGLDM matrix. The difference vector relates to the number of occurrences SGLDM entries differ by a value $k = |i - j|$ ranging from 0 to N. The difference vector is used in the computation of features F9 and F10 given by equations (4.15) and (4.16).

$$p_{(x-y)}(k) = \sum_{i=1}^{N} \sum_{j=1}^{N} p_{(x-y)}(i) log[p_{(x-y)}(i)] \quad where \quad k = |i - j| \tag{4.14}$$

Difference Variance: Equation (4.15) calculates the variance of entries in the difference vector in (4.14).

$$\begin{aligned} \textit{Difference Variance:} \quad F_9 &= \sum_{i=1}^{N} (i - F_9^{'})^2 \cdot p_{(x-y)}(i) \\ \textit{And} \quad F_9^{'} &= \sum_{i=1}^{N} i \cdot p_{(x-y)}(i) \end{aligned} \tag{4.15}$$

Difference Entropy: Equation (4.16) calculates the entropy of entries in the difference vector in (4.14).

$$\textit{Difference Entropy:} \quad F_{10} = -\sum_{i=1}^{N} p_{(x-y)}(i) log(p_{(x-y)}(i)) \tag{4.16}$$

Information Measures of Correlation: Equation (4.17) calculates the information measures of correlation feature which is a statistical metric developed from the sums of row i and column j entries of the SGLDM.

$$\begin{aligned} \textit{Information Measures of Correlation:} \quad F_{11} &= (1 - exp[-2(HXY2 - HXY)]^{1/2}) \\ Where, \quad HXY2 &= -\sum_{i=1}^{N}\sum_{j=1}^{N} p_x(i) p_y(j) log(p_x(i) p_y(i)) \\ HXY &= -\sum_{i=1}^{N}\sum_{j=1}^{N} p_{(d,\theta)}(i,j) log(p_{(d,\theta)}(i,j)) \\ p_x(i) &= \sum_{j=1}^{N} p_{(d,\theta)}(i,j) \\ p_y(j) &= \sum_{i=1}^{N} p_{(d,\theta)}(i,j) \end{aligned} \tag{4.17}$$

4.3 Analysis of SGLDM Features from Thermally Deteriorated Kraft Paper

For the set of thermally deteriorated winding insulation paper samples described in Chapter 3, forty images of each aging class (0, 120, 250, and 400-hours at 140°C) have been converted to forty feature vectors per aging class using the SGLDM method described in Section 4.2. Each feature vector contains 22 texture features obtained from (4.5)-(4.17) based on SGLDM matrices developed in two orientations; vertical and horizontal. These features will be analyzed in the subsections 4.3.1 and 4.3.2. Firstly, feature sensitivity will be evaluated to determine how substantially the feature values change between aging classes. Secondly, feature values will be analyzed by correlating the features with aging class information and degree of polymerization measurements on the thermally aged paper samples.

4.3.1 Statistical Texture Feature Sensitivity Evaluation

To analyze sensitivity of the SGLDM texture features as metrics for discerning between differing levels of deterioration, Fisher Discriminant Ratios (FDR) have been applied to individual texture features to measure feature differences between aging classes. Fisher Discriminant Ratios are a linear measure commonly used for discriminating between to statistical variables or data sets [72]. The formula for calculating the Fisher Discriminant Ratio is given in (4.18),

$$FDR = \frac{(\mu_1 - \mu_2)^2}{\sigma_1^2 + \sigma_2^2} \tag{4.18}$$

where μ_1 and μ_2 represent the mean of the two data sets respectively, and σ_1 and σ_2 are the standard deviations of the data sets.

Prior to computing the feature FDR values using (4.18), the features were normalized using (4.19). The feature value x is normalized to $\bar{x}$ by subtracting the global mean $\mu_{x_{global}}$

(average of all classes) and dividing by the feature global standard deviation.

$$\bar{x} = \frac{x - \mu_{x_{global}}}{\sigma_{x_{global}}} \tag{4.19}$$

Normalization is necessary because some features have magnitude ranges greater than others and without normalization these features would have disproportionately larger FDR. After normalization the computed the FDR values may be compared directly between features.

To evaluate the sensitivity of individual SGLDM features, the FDR was computed for each class comparison (0-to-120, 120-to-250, 250-to-400, 0-to-250, 0-to-400, and 250-to-400) and averaged. By computing the average FDR per feature, it will show which SGLDM texture features are the most sensitive to detecting surface morphological changes caused from thermal deterioration.

The average FDR values for each SGLDM feature are ranked in order of highest to lowest sensitivity in Tables 4.1 and 4.2, representing features computed using minimum-maximum normalization and histogram equalization, respectively. The feature values for minimum maximum normalization on average have higher FDR than histogram equalization. This is due to histogram equalization causing a more dramatic change to the pixel intensity values in the original sample images to the extent that some texture information may be lost. It is also noteworthy that some features are significantly impacted by the image preprocessing method. The feature sum-average ranked near the top in sensitivity when using minimum maximum normalization but is near the bottom when using histogram equalization.

The entropy feature, expressed in (4.13), has the highest FDR among SGLDM features for both image preprocessing methods. This suggests that entropy (4.13) is the most sensitive SGLDM feature to changes in the paper surface morphology from thermal deterioration. The inverse difference moment feature (4.8) also yields relatively high FDR values in both preprocessing methods.

Table 4.1. Average Fisher Discriminant Ratio from all class comparison on winding paper insulation image set preprocessed using minimum maximum normalization.

Feature Name	Feature Number	Averge FDR between all class comparisons
Entropy	F8 & F19	30.14
Inverse Difference Moment	F4 & F15	22.63
Sum Average	F5 & F16	22.19
Difference Entropy	F10 & F21	20.20
Contrast	F2 & F13	18.25
Sum Variance	F6 & F17	17.00
Angular Second Moment	F1 & F12	14.84
Sum Entropy	F7 & F18	14.34
Difference Variance	F9 & F20	11.36
Variance	F3 & F14	9.39
Information Measures of Correlation	F11 & F22	1.58

Table 4.2. Average Fisher Discriminant Ratio from all class comparison on winding paper insulation image set preprocessed using histogram equalization normalization.

Feature Name	Feature Number	Averge FDR between all class comparisons
Entropy	F8 & F19	19.61
Angular Second Moment	F1 & F12	9.40
Sum Entropy	F7 & F18	8.73
Inverse Difference Moment	F4 & F15	7.63
Difference Entropy	F10 & F21	2.55
Information Measures of Correlation	F11 & F22	1.53
Difference Variance	F9 & F20	1.52
Contrast	F2 & F13	1.15
Variance	F3 & F14	0.80
Sum Average	F5 & F16	0.17
Sum Variance	F6 & F17	0.03

4.3.2 Correlation of SGLDM Features to Degree of Polymerization

The SGLDM features for entropy and IDM showed strong sensitivity to changes in thermal deterioration level in Section 4.3.1. In this section, the correlation between these SGLDM features and DP will be analyzed. The purpose of this analysis will be to observe how the statistical texture feature values trend in relation to aging.

In Fig. 4.3, the top graph shows the relationship between the SGLDM feature for entropy and DP. The four data points pertain to the aging levels at 0, 120, 250, and 400 hours of deterioration at 140°C. Vertical bars in the graph indicate 95% confidence limits for the variance in feature entropy. Horizontal error bars for DP measurement are not available because the number of samples evaluated for DP are too few to evaluate statistical confidence limits. However, the laboratory which performed the DP measurements estimate less than 2% error in measurement. Figure 4.3 shows that as deterioration of the paper sample increases (*i.e.* direction of reducing DP) the statistical texture entropy reduces.

Recall that in Section 4.2.1, the texture feature for entropy was defined as a measure of the disorder an texture image. The trend for entropy implies that as the paper becomes increasingly deteriorated from thermal stress, that the surface texture of the paper would becomes more orderly; or in other words, homogeneous. In Fig. 3.6, microscopic images of new condition paper show well-defined fibers, interwoven in a network. As the paper becomes more deteriorated, the fiber walls breakdown, the fibers become thinner. Overall the breakdown of fibers makes the texture of deteriorated appear more uniform or homogeneous. From these observations it is logical that the entropy feature reduces as the paper becomes more thermally deteriorated.

Opposite to entropy, the relationship between IDM to DP increases with increasing deterioration as shown in Fig: 4.4. This relationship is also logical when drawing comparisons to the images of deteriorated paper samples in Fig. 3.6. Because IDM is a measure of the local homogeneity in an image we see an increasing trend in IDM as the paper samples

(a)

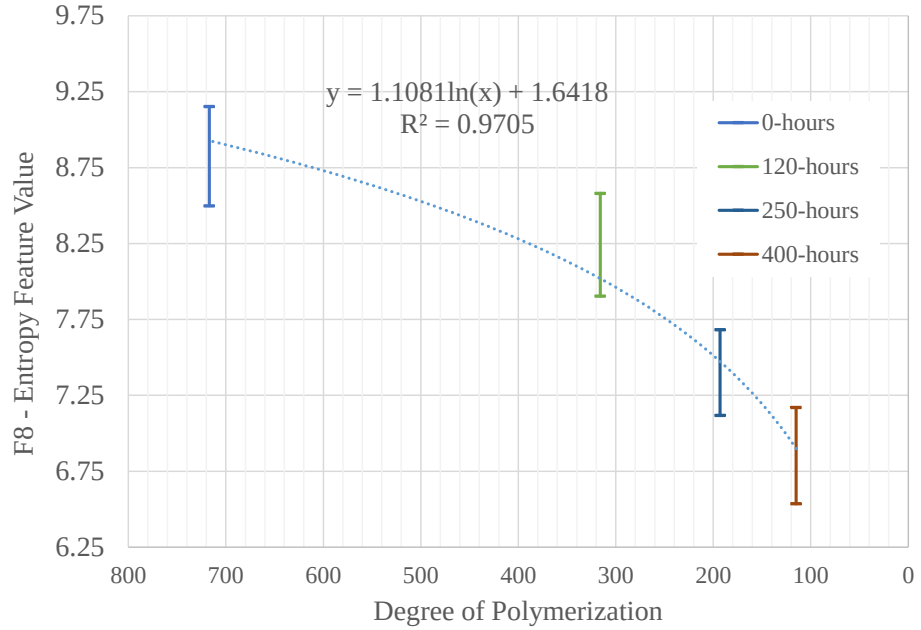

(b)

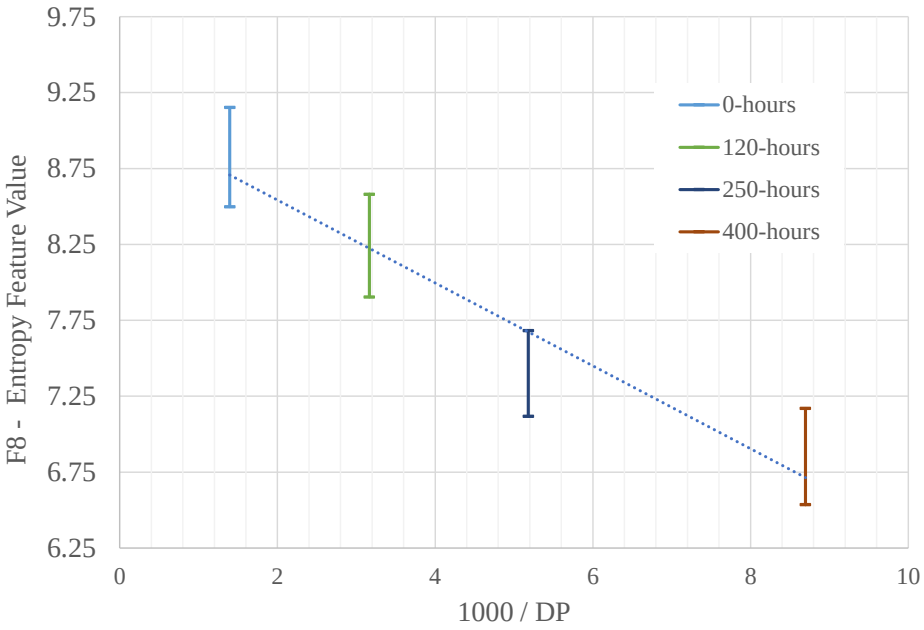

Fig. 4.3. Correlation between SGLDM Entropy Feature and DP.In (a) a logarithmic curve relationship between Entropy and DP is shown. In (b) a linear relationship is visble with the horizontal axis plotted as 1000/DP.

(a)

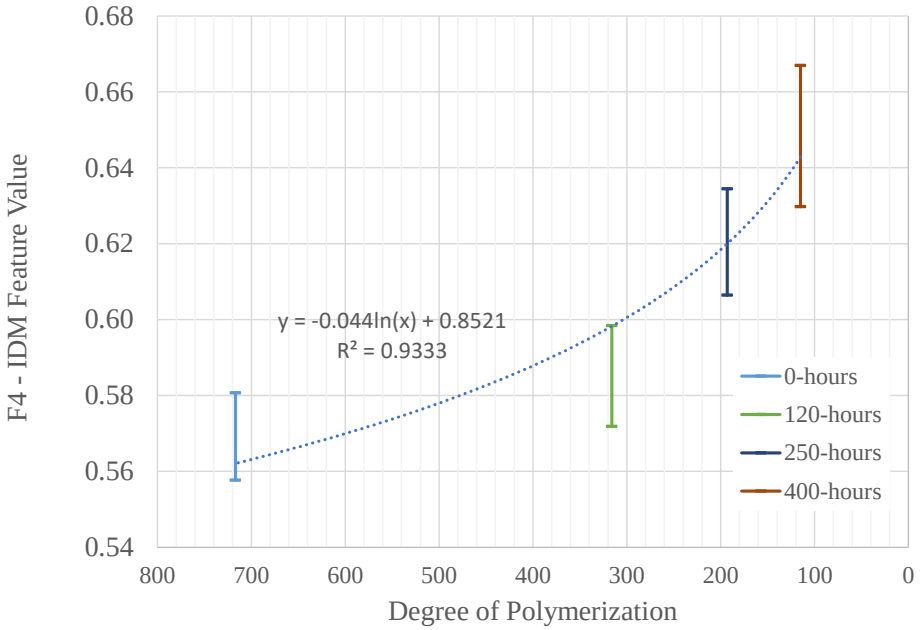

(b)

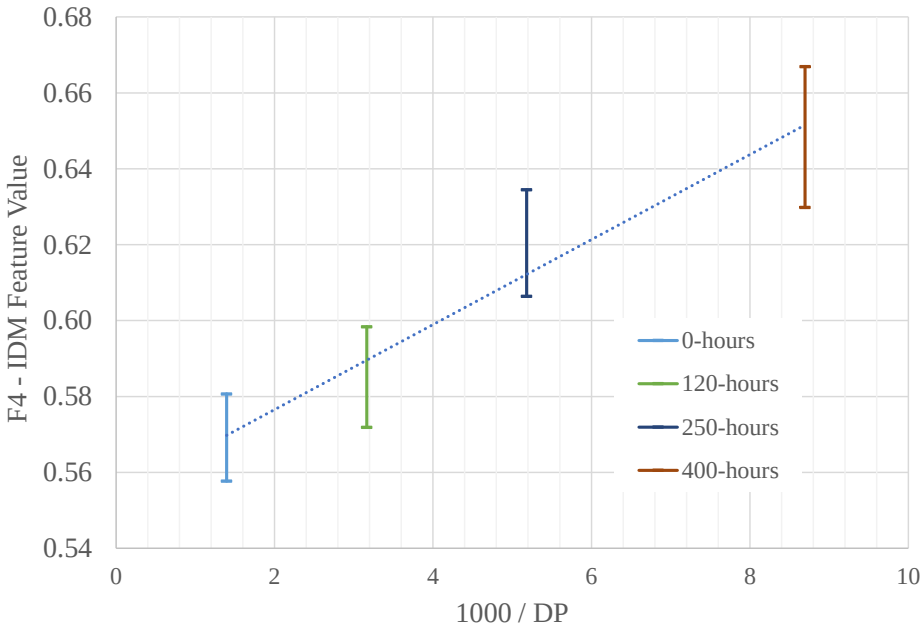

Fig. 4.4. Correlation between SGLDM IDM Feature and DP. In (a) a logarithmic curve relationship between IDM and DP is shown. In (b) a linear relationship is visble with the horizontal axis plotted as 1000/DP.

become more homogeneous in appearance due to deterioration.

Both entropy and IDM features appear to show logarithmic relationships with DP. In Fig. 2.3 it was shown that a similar logarithmic relationship exists between tensile strength and DP. Recall from Fig. 2.3 that a linear relationship exists between tensile strength and a factor of 1000/DP. A similar linear relationship is be observed for entropy and IDM in the bottom graphs of Fig. 4.3(a) and Fig. 4.4(b). This information strongly suggests that the entropy and IDM are directly proportional to tensile strength of the paper. Proportionality of entropy to tensile strength is shown directly in Fig. 4.5 where entropy is plotted versus tensile strength based on data obtained from [42] and [43]. It is clear from Fig. 4.5 that tensile strength and entropy are proportional to one another because their correlation fits a straight line graph.

The observation that statistical texture features are directly proportional to the tensile strength of paper is significant because it suggests that the characteristics about paper surface morphology may be used to estimate deterioration level. Unfortunately, because the confidence limits for entropy in Fig. 4.3 and 4.4 are overlapped between aging classes, logarithmic expressions obtained from the best fit curves would yield high error when attempting to use them for direct estimation of the deterioration level. In the next section, the complete feature set will be analyzed with the use of machine learning techniques to develop a classifier for more accurate estimation of deterioration level.

4.4 Automated Classification of Deterioration using SGLDM Features

In the previous section, we observed that a few of the SGLDM features trend proportionately with tensile strength. Large variance in the feature values for a given tensile strength (or DP) make the use of individual features for estimation of deterioration level inaccurate. In this

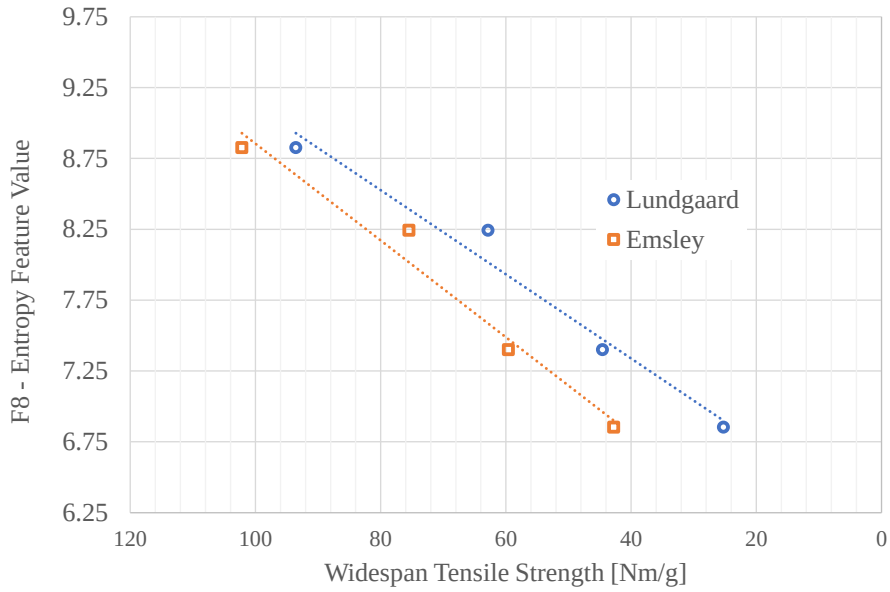

Fig. 4.5. Entropy Feature as a function of Tensile Strength. Correlation obtained from empirical data relating DP and Tensile Strength from [42] and [43].

section, we will combine the SGLDM features with standard machine learning techniques to construct a statistical classifier that will more accurately estimate the deterioration level of thermally aged paper from microscopy images. Two standard methods of machine learning have been used to train statistical classifiers, Linear Discriminant Analysis (LDA) and Principal Component Analysis (PCA).

Linear Discriminant Analysis is a supervised learning method, meaning that the classifier is trained with the information of which class each training sample belongs [72]. The classifier is designed to maximize the separation between classes. The final classifier is represented mathematically as a linear combination of the original feature set that applies weight (emphasis) on features in the feature space that will maximize the separation between classes.

Principal Component Analysis (PCA) is categorized as an unsupervised learning method, meaning that the classifier is trained without knowledge of the class that each sample belongs to. Instead, the classifier works by maximizing the total statistical variance available in the set of sample data [72]. Similar to LDA the final classifier is a linear combination of the original feature set, but PCA applies weight to features such that all samples will be maximally separated from each other in the feature space.

The SGLDM texture features obtained from the original set of 40 sample images per aging class have been used to train the LDA and PCA classifiers. Separate classifiers have been trained for each image pre-processing method; minimum-maximum normalization and histogram equalization. To evaluate the classifiers, the k-NN nearest neighbor algorithm with k=5 neighbors was used [72]. Five neighbors is considered suitable for the size of the dataset, as k=3 neighbors was considered too few and susceptible to higher classification error rates, while k=7 is too large relative to the data set with contains only 40 sample images per class. Evaluation was carried out on an 'unseen' test data set of 70 sample images. These sample images were not used in the original classifier training. A second

evaluation was performed using leave-one-out cross-validation which applies the k=5 nearest neighbor algorithm on all training and test data points individually [72].

Two LDA classifiers were generated using training data, one using minimum-maximum normalization, and the other using histogram equalization. Both LDA classifiers were reduced to three LDA features each and the final projections of the training data onto the LDA feature spaces are shown in Fig. 4.6 and 4.7 for minimum-maximum normalization and histogram equalization respectively. The separation between aging classes in the minimum-maximum normalization feature space appears better than the histogram equalization space. Recall that histogram equalization corrects brightness variations in original sample images by rescaling the pixel intensity values to be evenly spread over the image. This has a dramatic effect on the sample images, and may have introduced some loss of texture information as compared to the minimum-maximum normalization classifier. In spite of some loss of class separation, the histogram equalization classifier in Fig. 4.7 still produces four distinctly separate classes. Because histogram equalization removes variations in brightness between sample images, it is clear that the classification is extracting differences in texture information.

For the PCA classifiers, the original feature set was reduced to five PCA features because five features were necessary to obtain at least 95% of the total variance from the original feature set. With greater than three features it is not possible to visualize the PCA classifier in its feature space as was done for LDA in Fig: 4.6 and 4.7.

Results from evaluation of the LDA and PCA classifiers are shown in table 4.3. The classifiers were evaluated using a set of 70-sample images that were not included in the original classifier training. As expected results for the LDA classifier produces lower classification error rates than the one trained using PCA. Observations about class separation in the LDA feature space being less for histogram equalization (Fig. 4.7) appear consistent with the classification error results. Histogram equalization error rates are higher for both

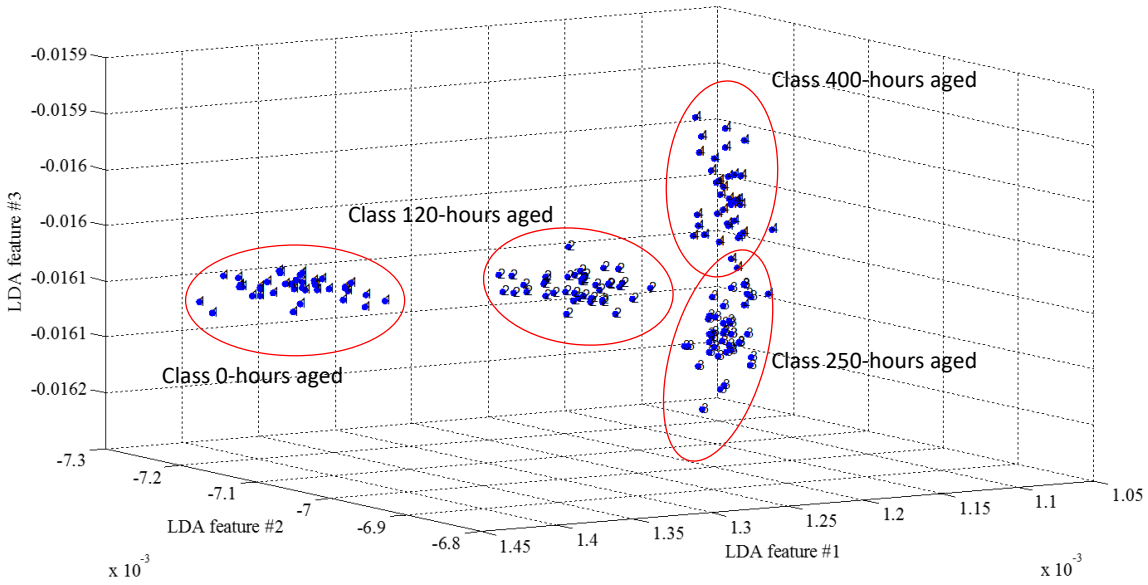

Fig. 4.6. Projection of SGLDM Features using LDA after being preprocessed by Minimum Maximum Normalization.

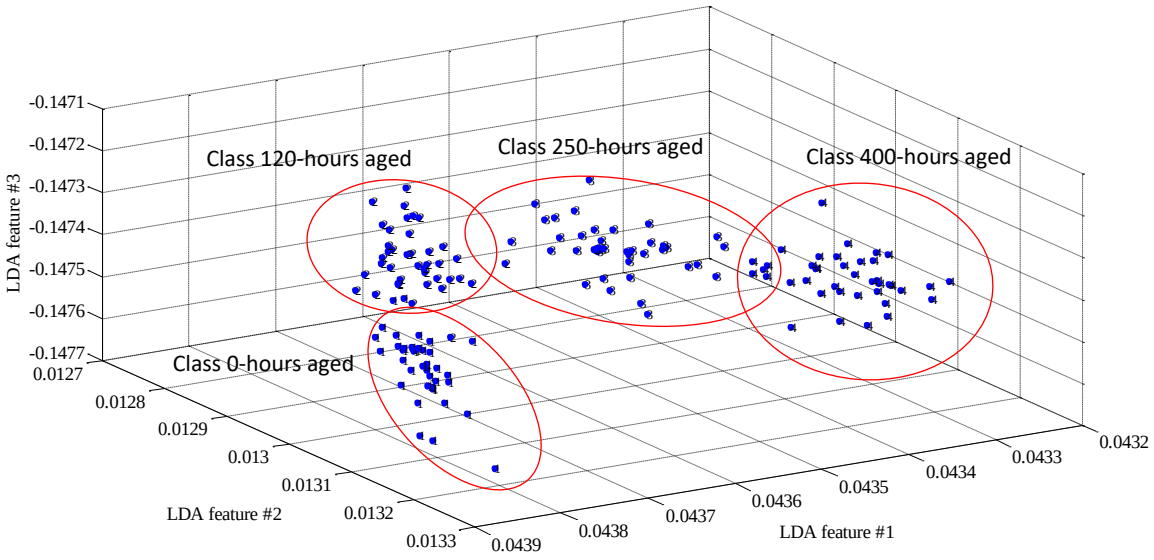

Fig. 4.7. Projection of SGLDM Features using LDA after being preprocessed by Histogram Equalization.

Table 4.3. Classification Error Summary for LDA and PCA classifiers from SGLDM Features. Errors computed separately for two different image normalization methods; Minimum-maximum and Histogram Equalization.

		Unseen Data Error Rate [%]	Cross Validation Error Rate [%]
Minimum Maximum Normalization	LDA	1.25	1.31
	PCA	1.25	2.18
Histogram Equalization	LDA	1.25	3.49
	PCA	2.50	6.11

LDA and PCA classifiers.

The worst case error rates occur when the classifier is generated from histogram equalization image preprocessing and using PCA at 2.50% for unseen data, and 6.11% for cross-validation. These are still relatively good in performance and from these results we can infer that the textural differences between paper aging classes are significant. For the type of paper thermally deteriorated in experiments the deterioration level may be estimated in one of the four aging classes with good accuracy.

4.5 Chapter Summary

To address the issues related to the darkening of thermal aged kraft paper samples caused by staining from oxidized oil, minimum-maximum and histogram equalization image preprocessing is applied to the microscopic images of thermally aged paper. Minimum maximum normalization improves contrast in te darkened images by extending the pixel intensity val-

ues over the full available range while histogram equalization redistributes the pixel intensity values equivalently over the range.

After image preprocessing, the SGLDM transform is applied to the sample images. The SGLDM converts images into a histogram based matrix that contains information about the pixel intensity values in the original image and their spatial arrangement in the image. Texture features are obtained from mathematical operations performed on the SGLDM matrix. In this thesis, a total of 22 statistical texture features are extracted from each paper sample image.

Analysis of the statistical texture features revealed that features for entropy and inverse difference moment (IDM) appear to be the most sensitive to changes in thermal deterioration level (aging class). When correlated to DP measurements, entropy and IDM texture features appear to trend logarithmically with degree of polymerization. In the case of entropy, the logarithmic relationship resembles the relationship between DP and tensile strength of paper. These findings suggest that there exists a relationship between the surface morphology of the paper quantified through statistical texture analysis with mechanical tensile strength properties of the paper.

The SGLDM statistical texture features can be manipulated using machine learning methods for automated classification and estimation of deterioration level. Classifiers developed using supervised learning algorithms (LDA) and unsupervised learning algorithms (PCA) yield low estimates for classification error rate. These results are promising, and suggest that the textural differences between aging classes are significant and well separated by classification.

Chapter 5

Transform-Based Texture Analysis of Thermally Deteriorated Paper using the Two-Dimensional Wavelet Transform

In this chapter, images of thermally deteriorated transformer winding insulation paper will be analyzed using a Wavelet Texture Analysis Method. Background on the wavelet transform and its expansion to two dimensions for the application of analyzing images will be discussed. A methodology for feature extraction from the wavelet transform sub-images will be described. Feature analysis and evaluation will be carried out in the same manner as was done for the SGLDM method in Chapter 4; sensitivity of the feature changes caused by thermal deterioration will be evaluated using Fisher Discriminant Ratios and a correlation between the wavelet texture features to degree of polymerization measurements will be analyzed. Lastly, unsupervised and supervised machine learning techniques will be applied to the wavelet texture features to evaluate the suitability of this method for automated

classification and estimation of thermal deterioration in transformer paper insulation.

5.1 Wavelet Texture Analysis

5.1.1 Discrete Wavelet Transform

The discrete wavelet transform is a mathematical operation that translates a function or signal into a linear combination of special basis functions called wavelets. One of the distinguishing features of the wavelet transform is that it retains spatial and frequency information from the original signal after transformation. The characteristic of retaining spatial information is what distinguishes the Wavelet transform from the Fourier Transform; retains only the frequency information [73].

The discrete wavelet transform representation of a one-dimensional discrete signal $f(n), n = 1, ..., M$ is given by (5.1) [68]:

$$f(n) = \frac{1}{\sqrt{M}} \sum_{k} C_{\phi}(j_0, k)\phi_{j_0,k}(n) + \frac{1}{\sqrt{M}} \sum_{j=j_0}^{\infty} \sum_{k} D_{\psi}(j, k)\psi_{j,k}(n). \tag{5.1}$$

In (5.1), the signal $f(n)$ is expressed as a linear combination of shifted and dilated basis functions given by $\phi_{j,k}$ and $\psi_{j,k}$. The scaling and shifting of these basis functions is expressed in:

$$\phi_{j_0,k}(n) = 2^{j/2}\phi(2^{j/2}n - k) \tag{5.2}$$

$$\psi_{j,k}(n) = 2^{j/2}\psi(2^{j/2}n - k), \tag{5.3}$$

where the parameter j dilates (stretches) the basis function and k shifts the basis function position relative to the original signal $f(n)$. The value j_0 is a default starting scale. $C_{\phi}(j_0, k)$ and $D_{\psi}(j, k)$ represent the scaling and wavelet coefficients in the linear combination shown in (5.1). These coefficients are computed from the convolution of the basis functions, $\phi_{j,k}$

and $\psi_{j,k}$, with the original signal $f(n)$. This convolution is expressed by the inner product equations given by:

$$C_\phi(j_0, k) = \frac{1}{\sqrt{M}} \sum_n f(n)\phi_{(j,k)}(n) \tag{5.4}$$

$$D_\psi(j, k) = \frac{1}{\sqrt{M}} \sum_n f(n)\psi_{(j,k)}(n). \tag{5.5}$$

The scaling and wavelet basis functions ϕ and ψ have some unique characteristics. Wavelets can have a variety of different waveshapes, but their waveshape must satisfy certain criteria. The wavelet ψ must have finite length, it must have zero mean, and it must be orthogonal to its scaling function ϕ [73]. Therefore, each wavelet ψ will have its own unique corresponding scaling function ϕ.

When convolved with the original signal $f(n)$ as expressed in (5.4) and (5.5), the scaling function ϕ will extract a low frequency approximation of $f(n)$, while ψ will extract the high frequency contents or the details. In this manner, the two basis functions act as digital filters, where convolution with the wavelet function ψ is a high-pass filter operation and convolution with the scaling function ϕ is a low-pass filter operation.

5.1.2 Wavelet Transform in Two Dimensions

When applying the wavelet transform to images, the image is treated as a two-dimensional signal $f(x, y)$ and convolution of the basis functions is applied to the rows (x) and columns (y) of the image in the combinations expressed by:

$$\phi(x, y) = \phi(x) \cdot \phi(y) \tag{5.6}$$

$$\psi^H(x, y) = \psi(x) \cdot \phi(y) \tag{5.7}$$

$$\psi^V(x, y) = \phi(x) \cdot \psi(y) \tag{5.8}$$

$$\psi^D(x, y) = \psi(x) \cdot \psi(y). \tag{5.9}$$

The basis functions for dilation and translation in two dimensions are represented by:

$$\phi_{j,m,n}(x,y) = 2^{j/2}\phi(2^j x - m, 2^j y - n) \tag{5.10}$$

$$\psi^i_{j,m,n}(x,y) = 2^{j/2}\psi(2^j x - m, 2^j y - n), \quad Where \quad i = \{H, V, D\} \tag{5.11}$$

The superscript i in (5.11) applies to the convolution combinations of basis functions referenced in (5.6)-(5.9) to obtain either horizontal, vertical or diagonal details.

Finally, the coefficients for the approximation image and detail sub-images are given by:

$$C_\phi(j,m,n) = \frac{1}{\sqrt{MN}} \sum_{x=0}^{M-1} \sum_{y=0}^{N-1} f(x,y) \cdot \phi_{j,m,n}(x,y) \tag{5.12}$$

$$D^i_\psi(j,m,n) = \frac{1}{\sqrt{MN}} \sum_{x=0}^{M-1} \sum_{y=0}^{N-1} f(x,y) \cdot \psi^i_{j,m,n}(x,y) \tag{5.13}$$

5.1.3 Discrete Wavelet Transform of Images

A schematic representation of the two-dimensional wavelet transform applied to an original image of size $M \times N$, is shown in Fig. 5.1. In the first stage of the transform, a convolution is performed between the basis functions ϕ and ψ and the rows of the image. The convolution effectively applies low-pass and high-pass filtering along the rows in image. In the following stage of the transform, rows are then down-sampled (decimated) which compresses the image horizontally. The decimation is analogous to the dilation of the basis functions by increasing decomposition depth j. At this stage of the transformation, the original image has been decomposed into two sub-images sized $\frac{M}{2} \times N$, with one sub-image containing approximate or low-frequency row information and the other containing detail or high-frequency row information from the original image.

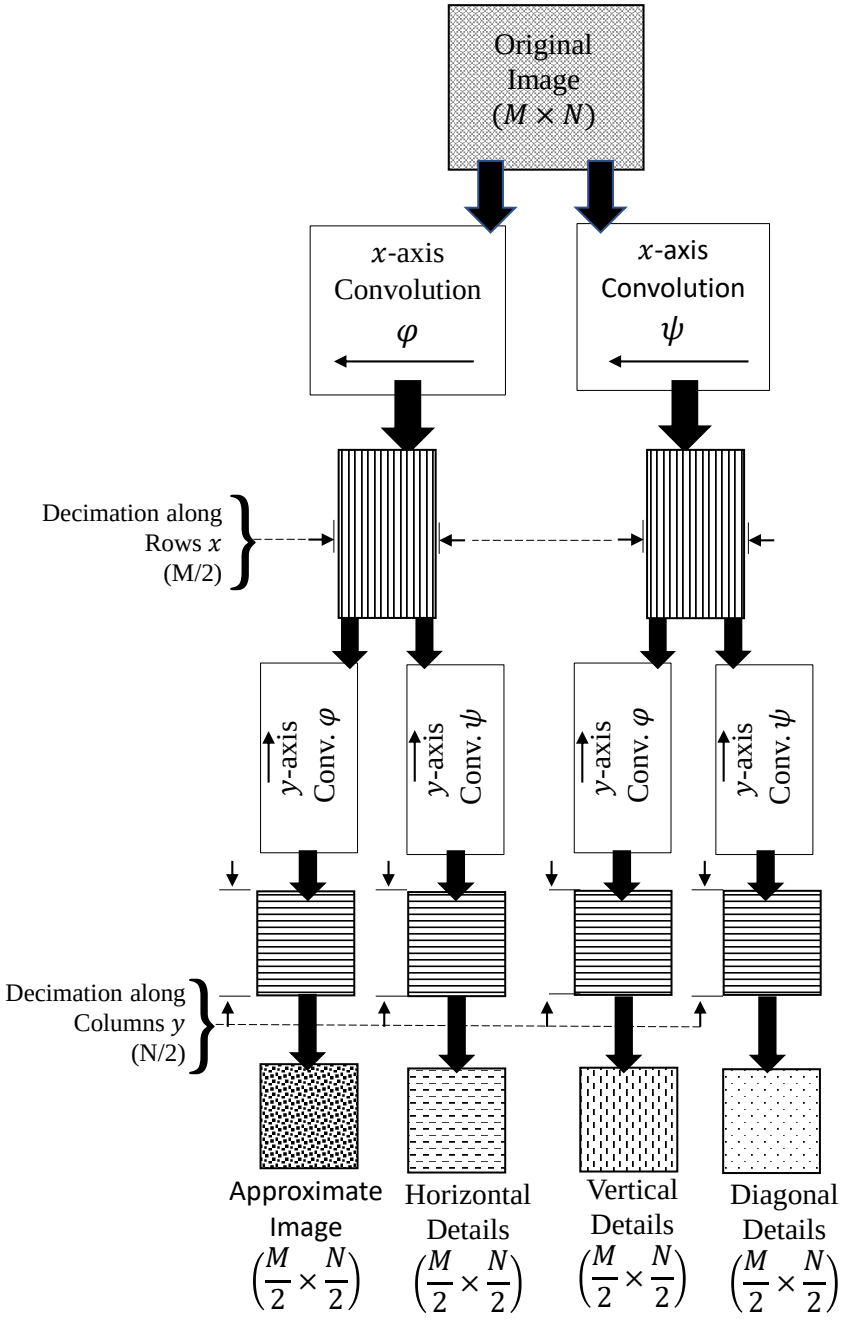

Fig. 5.1. Schematic representation of two-dimensional wavelet transform of an image.

In the following stage, each of the horizontally compressed sub-images from the previous step are convolved (filtered) by the basis functions ϕ and ψ along the columns to extract low-pass and high-pass image information along the columns. Following the convolution, now columns are down-sampled (decimated). The final result from the Wavelet Transform is four separate sub-images sized $\frac{M}{2} \times \frac{N}{2}$; one is corresponding to an approximation of the original image, that contains only low-frequency content. The three remaining sub-images contain detail information from the original image in the horizontal, vertical, and diagonal orientations.

Successive decompositions using Wavelet Transform on images are manipulated by re-inserting the approximate image from Fig. 5.1 back in as the original, and repeating the transform process. In doing so, the detail information can be extracted at lower resolutions.

5.2 Wavelet Texture Analysis Method Implementation

5.2.1 Selection of Wavelet Type

The wavelet chosen for texture analysis of thermally deteriorated paper sample images is the Daubechies 4 wavelet [74]. The discrete waveform for Daubechies 4 is shown in Fig. 5.2. Daubechies 4 wavelet is an orthogonal wavelet. It was chosen for the texture analysis on microscopic images paper samples because it is appropriately sized for the sizes of texture details in the images of paper samples. From the microscopic images of thermally-deteriorated paper samples shown in Chapter 3, the approximate width of smallest paper fibers are estimated in the range of 10-12 pixels wide. The Daubechies 4 wavelet has a support length of eight, making it is small enough to extract details as small the fibers imaged for texture analysis.

Another reason that the Daubechies 4 Wavelet was chosen over other wavelet types is because it's wavelet basis function waveshape contains sharp transitions. These sharp tran-

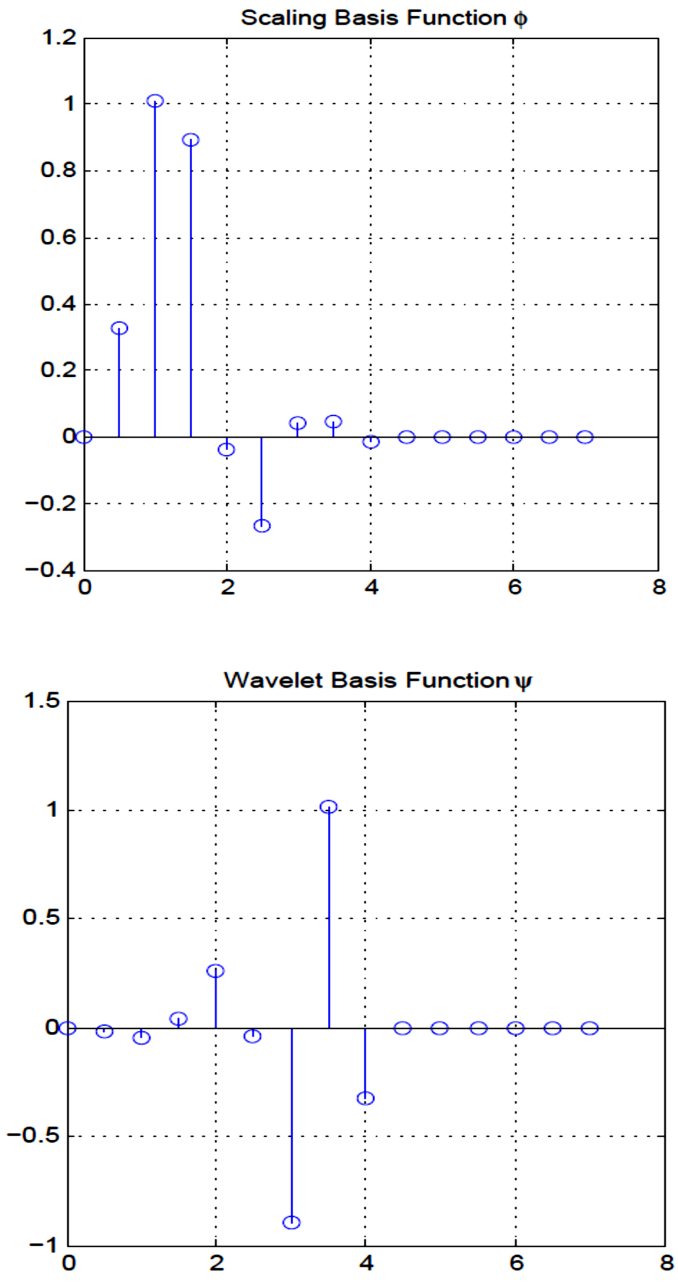

Fig. 5.2. Discrete form of the Daubechies 4 scaling and wavelet basis functions.

sitions are useful for analyzing microscopic images of thermally-deteriorated paper samples because sharp transitions occur at fiber edges and at sites of cracks or fissures in the paper caused from thermal deterioration.

5.2.2 Decomposition depth

The decomposition depth used for texture analysis depends on the size of the original image. With successive decompositions the residual approximation image becomes smaller and smaller in size and at some level the residual texture information becomes negligible. For the microscopic images of thermally-deteriorated paper shown in Chapter 3, the original images are sized 1600×1200. Because wavelet decompositions are normally performed with signal sized by a factor of two, (2^j), the sample images were cropped to a size 1024×1024 and the number of decompositions used was limited to four levels ($j = 4$). After four decomposition levels the residual approximate image is reduced to a size of 64×64. Past this level ($j = 4$) very little texture information remains to be extracted, and at this decomposition stage the wavelet dilation is equivalent to $1/8^{th}$ of the original image width and height.

5.2.3 Image Boundary Treatment for Convolution

Because the computation of wavelet transformed images involves convolution of rows and columns in the image with a wavelet and scaling basis functions which have finite length, border distortions will occur at the edges of the image where the Wavelet extends past the image boundary. When the wavelet transform is applied recursively to the approximation coefficients, border distortion can create artificial details that would introduce errors in the detail coefficient computation in successive decompositions.

To limit the influence of border distortions in calculation of the detail coefficients, a method called symmetric boundary extension has been applied with the two-dimensional

wavelet transformation. Symmetric boundary extension, extends the original image by adding a reflection of the rows and columns at the edge of the image. The length of this extension is eight-rows and eight-columns to accommodate the Daubechies 4 Wavelet length in convolution. Because texture in the original paper sample images are uniform over the entire image, symmetric boundary extension will have little effect on the analysis of texture detail because the added image content is expected to be similar as everywhere else in the image.

5.2.4 Extraction of Wavelet Texture Features

Wavelet features are generated by first converting the paper images into gray-scale by the same method mentioned in Section 4.1 and cropping them to size 1024×1024 as mentioned in Section 5.2.2. The two-dimensional wavelet transform is applied down to four decompositions levels ($j = 4$) using the Daubechies 4 wavelet. Finally statistical texture features of the paper sample images were computed by performing mathematical operations on the detail coefficient matrices D_{ψ}^{i} from the Wavelet Transform. A total of twelve (12) detail coefficient matrices will be generated from $j = 4$ decompositions. Note that all of the texture information is contained in the detail coefficients therefore no features are extracted from the approximation coefficients. The approximation coefficients only carry information about tonal variation in the sample images.

Two mathematical operators have been selected for converting the detail coefficient matrices D_{ψ}^{i} into a single numerical parameter. The first operator formula is the l_{norm}^{1}:

$$l_{norm}^{1} = \frac{1}{M \cdot N} \sum_{m=1}^{M} \sum_{n=1}^{N} |D_{\psi}^{i}(m,n)| \tag{5.14}$$

which computes the sum of the absolute value of the detail coefficients. The second mathematical operator is energy:

$$Energy = \frac{1}{M \cdot N} \sum_{m=1}^{M} \sum_{n=1}^{N} [D_{\psi}^{i}(m,n)]^2, \tag{5.15}$$

which is computed as the sum of squares of the detail coefficients. Both feature values are normalized by the number of cells in the detail coefficient matrix.

5.3 Analysis of Wavelet Texture Analysis Results

In Fig. 5.3, the results of two ($j = 2$) successive Wavelet Transform decompositions on two kraft paper sample images are shown. The format used for displaying the transformation where the sub-images are nested within the frame size of the original image, is a conventional method of displaying Wavelet transformations on images [14]. The quadrant sub-images display the Wavelet transform detail coefficients $D_{\psi}^{H,V,D}$ which are extracted from the original image in the first decomposition ($j = 1$) and recursively from the residual approximation image at higher decomposition levels ($j > 1$). The residual approximation coefficients are indicated by C_{ϕ}. Fig. 5.3a is the image of new-condition paper and Fig. 5.3b is that of the paper after 400-hours of thermal deterioration at 140°C. The brightly colored, speckled content in detail sub-images is shows texture detail at those regions of the original image.

Based on the brightness of the speckled content in Fig. 5.3b, it suggests that the amount of texture detail present in the new-condition sample is greater than the sample aged 400-hours at 140 °C. From this observation, we may expect the calculated $l1_{norm}$ (5.14) and *energy* (5.15) feature values to be greater for the new condition paper than the aged condition. Figure 5.3 also shows that there may be a relationship between the density of texture details and decomposition level.

In Fig. 5.4, the total average of the detail coefficient energies (5.15) are plotted as a function of decomposition level. Curves for each aging class (0, 120, 250, and 400-hours)

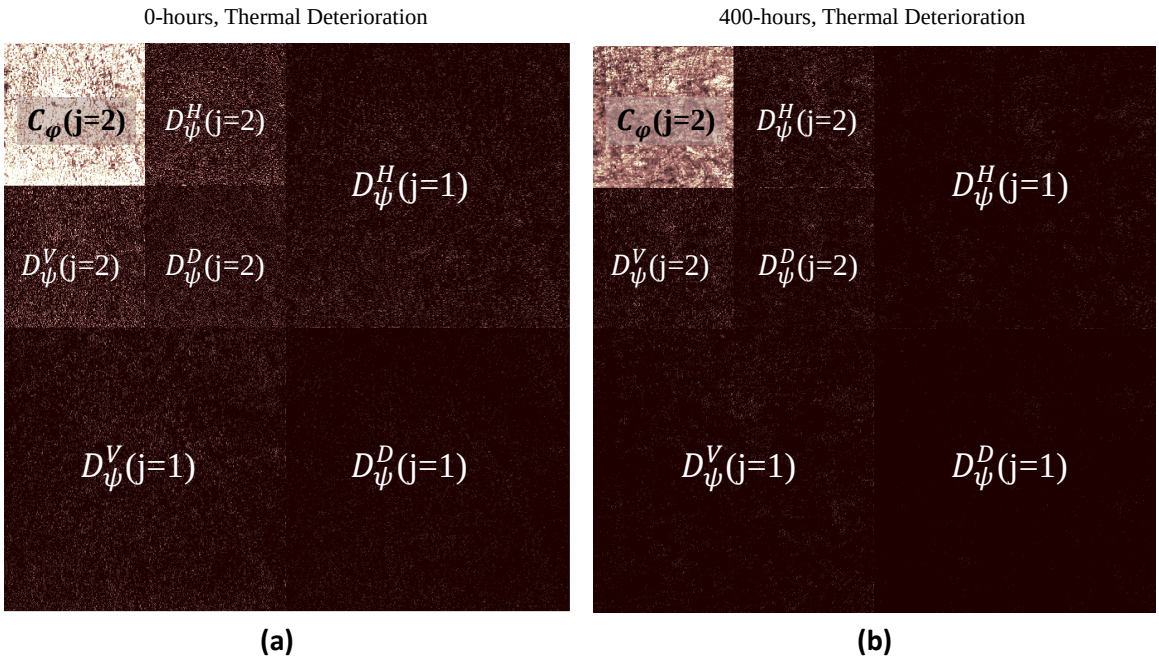

Fig. 5.3. A comparison of Wavelet decompositions ($j = 2$ levels) for thermally deteriorated paper samples (a) 0-hours at $140°$C on-left, and (b) 400-hours at $140°$C.

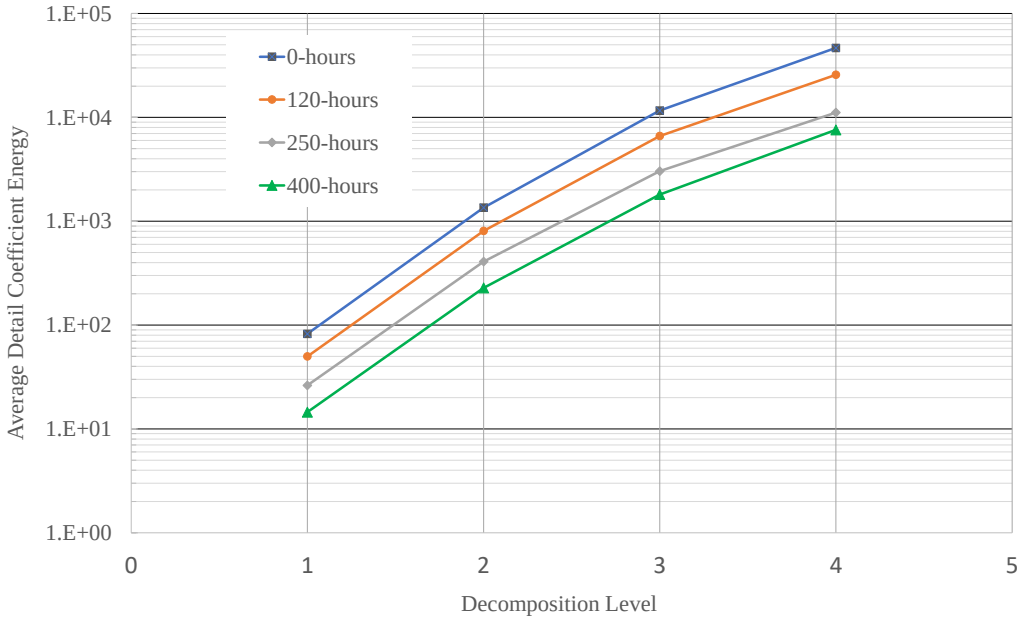

Fig. 5.4. Average detail coefficient energy (H,V, and D) as a function of decomposition level j.

are plotted independently. The vertical axis for the average detail coefficient energy is on a logarithmic scale. From Fig. 5.4, it appears that over four decomposition levels (j=1-4) the texture energy increases as a function of decomposition. This trend applies to each aging class. However, because this trend appears in all deterioration levels, i.e. (0, 120, 250, and 400 hours) we consider that the increase in energy as a function of decomposition level may be a function of the Wavelet Transform method and the selection of Daubechies 4 wavelet basis functions. Figure 5.4 also shows that the average texture detail energy reduces with increased thermal deterioration.

5.3.1 Wavelet Texture Feature Sensitivity Evaluation

Similar to the sensitivity analysis performed on the SGLDM features in 4.3.1, the wavelet texture features are evaluated using Fisher Discriminant Ratios (FDR) calculated between

Table 5.1. Average Fisher Discriminant Ratio from all class comparisons of Detail Coefficient $l1_{norm}$

Feature Name	Averge FDR between all class comparisons
Vertical Detail, decomp. j=4	45.24
Diagonal Detail, decom. j=4	29.30
Vertical Detail, decomp. j=3	21.21
Horizontal Detail, decomp. j=4	20.02
Diagonal Detail, decom. j=3	15.69
Horizontal Detail, decomp. j=3	14.16
Vertical Detail, decomp. j=2	11.78
Diagonal Detail, decom. j=2	10.00
Horizontal Detail, decomp. j=2	9.79
Diagonal Detail, decom. j=1	9.10
Horizontal Detail, decomp. j=1	8.58
Vertical Detail, decomp. j=1	7.99

Table 5.2. Average Fisher Discriminant Ratio from all class comparisons of Detail Coefficient $Energy$

Feature Name	**Averge FDR between all class comparisons**
Vertical Detail, decomp. j=4	26.09
Diagonal Detail, decom. j=4	22.35
Horizontal Detail, decomp. j=4	18.34
Vertical Detail, decomp. j=3	13.36
Horizontal Detail, decomp. j=3	13.07
Diagonal Detail, decom. j=3	11.62
Horizontal Detail, decomp. j=2	8.15
Vertical Detail, decomp. j=2	7.89
Diagonal Detail, decom. j=2	7.42
Diagonal Detail, decom. j=1	6.83
Horizontal Detail, decomp. j=1	6.80
Vertical Detail, decomp. j=1	5.59

the classes of 0, 120, 250, and 400-hours at 140°C. In total, there are five between-class FDR comparisons (0-to-120, 120-to-250, 250-to-400, 0-to-400, and 120-to-400). By computing the average FDR per feature, it shows which wavelet texture features are the most sensitive to surface morphological change caused by thermal deterioration.

In Tables 5.1 and 5.2, the average FDR values from the $l1_{norm}$ and *energy* features are shown, ranked in the order of their sensitivity to thermal deterioration. Results show that there is an increasing trend in feature sensitivity as the decomposition level j is increased. This means that the features obtained by computing the $l1_{norm}$ and *energy* of the wavelet detail coefficients will yield better discernibility between deterioration levels at high decomposition levels rather than the low ones (in the range from j=1-4).

5.3.2 Correlation Between Wavelet Texture Features and DP

Wavelet texture features for $l1_{norm}$ and *energy* of the detail coefficients are plotted as a function of the DP in Fig. 5.5 and 5.6, respectively. Note that the vertical axes in each figure are plotted on a log scale for better viewing.

The (a), (b), and (c) sub-figures in Fig. 5.5 show the $l1_{norm}$ of the horizontal, vertical, and diagonal details, respectively. Each individual data point in the figure represents the mean feature values with 95% confidence limits represented by the vertical error bars. The mean feature value and 95% confidence limits are obtained from processing forty sample images.

The general trend here again is that the *energy* and $l1_{norm}$ wavelet texture features increase with increasing the decomposition level j. It is also notable the the horizontal, vertical, and diagonal features in Fig. 5.5 and Fig. 5.6 each have similar characteristics when plotted as function of DP. For each feature, a best-fit polynomial (of an order of 2) has been fitted to the dataset's wavelet feature values.

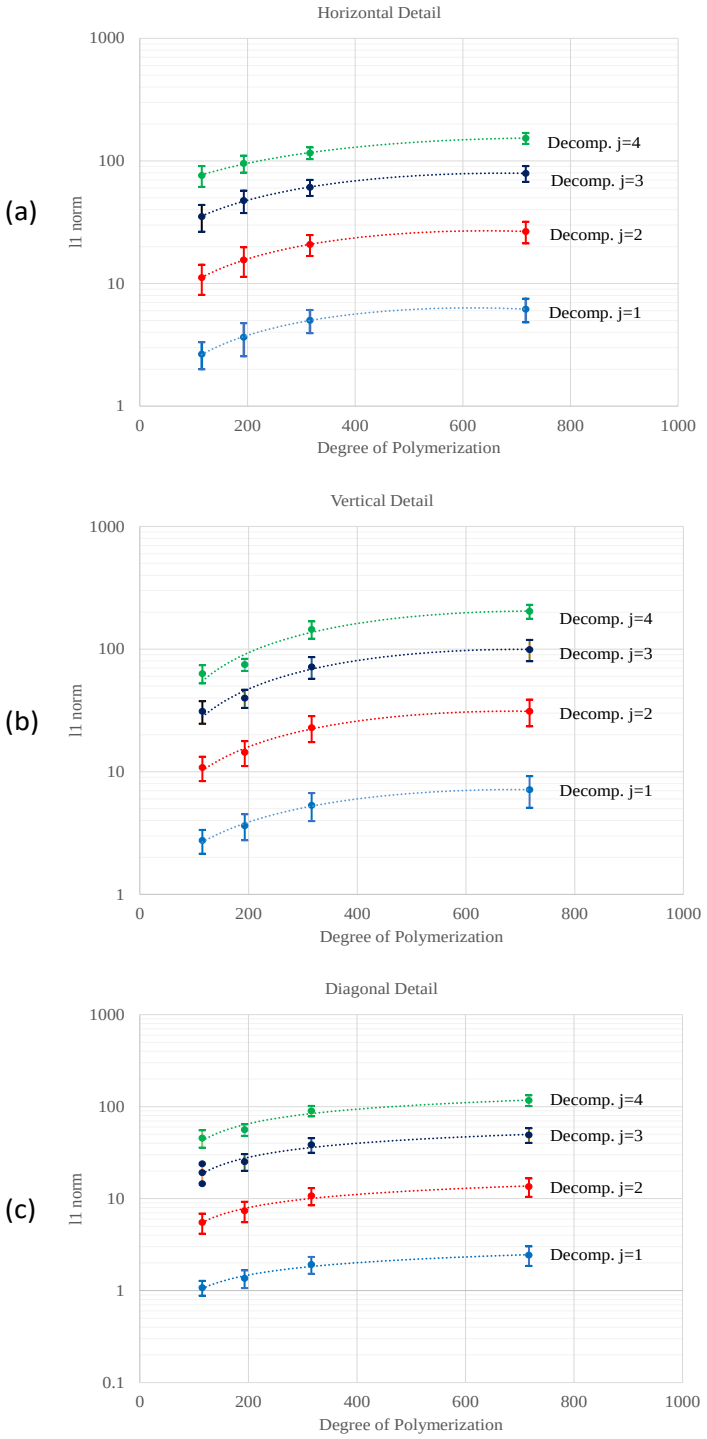

Fig. 5.5. Wavelet detail coefficient $l1_{norm}$ versus degree of polymerization.

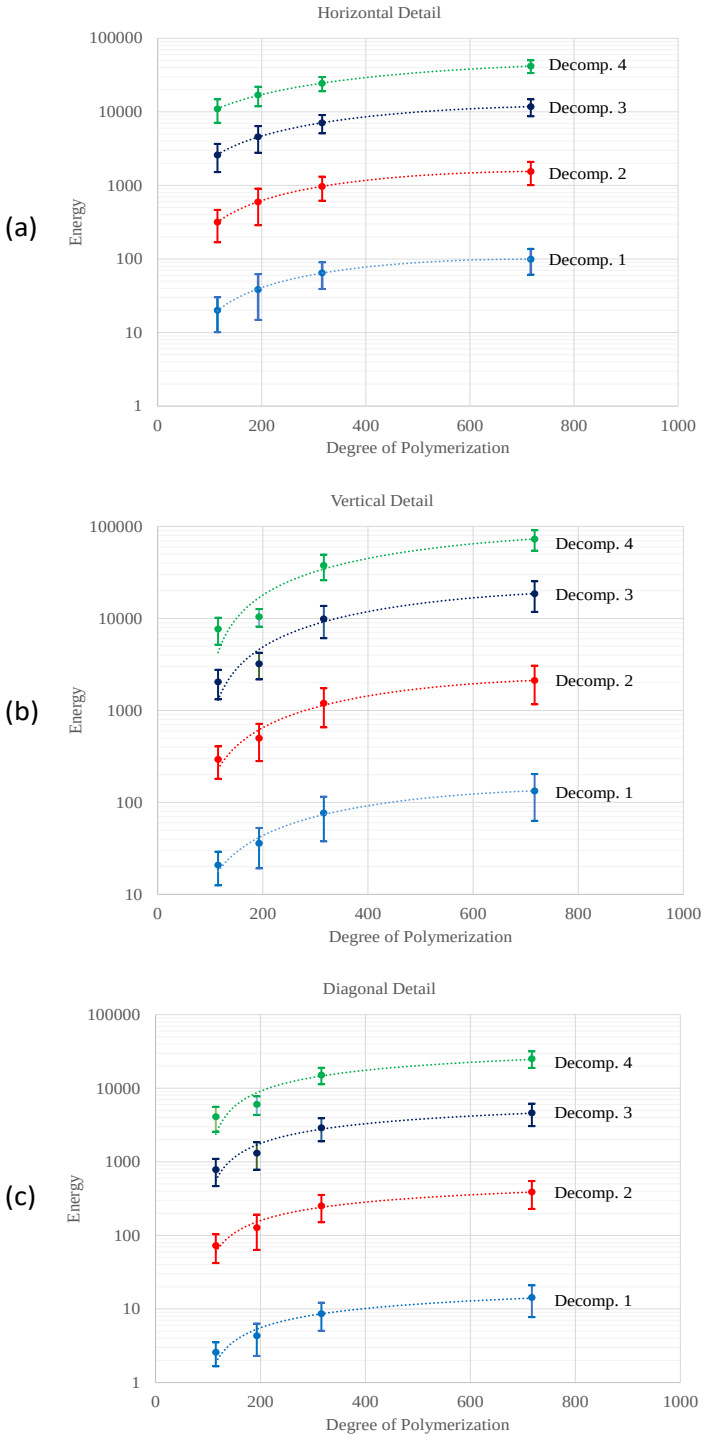

Fig. 5.6. Wavelet detail coefficient energies versus degree of polymerization.

5.3.3 Automated Classification of Thermal Aging Using Wavelet Texture Analysis

The wavelet texture features developed in Section 5.2 were used to train a classifier using LDA and PCA machine learning techniques. The training methods are the same that were used on features developed for the SGLDM Texture Analysis method in section 4.4. To evaluate the classifiers the k-NN nearest neighbor algorithm with k=5 nearest neighbors is used. The justification for k=5 nearest neighbors is the same as those that were stated in Section 4.4. Evaluation was carried out on an 'unseen' test data set of 70 sample images. These sample images were not used in the original classifier training. A second evaluation was performed using leave-one-out cross-validation which applies the k=5 nearest neighbor algorithm on all training and test data points individually.

The wavelet texture features obtained from the $l1_{norm}$ (5.14) and $energy$ (5.15) of the detail coefficients were used to generate two separate sets of LDA and PCA classifiers. The reason for not combining feature sets from $l1_{norm}$ and $energy$ into one large classifier is because the calculation of these features are too similar, and combining them would effectively create duplication of the same information in the classifier. Because computationally $l1_{norm}$ is simpler than $energy$, evaluation of both feature sets will at least indicate if there are some computational saving to be gained from using $l1_{norm}$ instead of $energy$ if their classifiers perform with similar classification errors.

The LDA classifiers for $l1_{norm}$ and $energy$ features, reduce the original set of 12 Wavelet features per sample image to three features. Projections of the thermal deteriorated paper sample image data into the LDA feature space are shown in Fig. 5.7 and 5.8 for $l1_{norm}$ and $energy$ classifiers respectively.

Figures 5.7 and 5.8 show that both $l1_{norm}$ and $energy$ feature spaces obtain good separation between aging classes. This is corroborated by low classification error results in Table 5.3 where the $l1_{norm}$ LDA classifier obtains 'unseen' data and cross-validation error

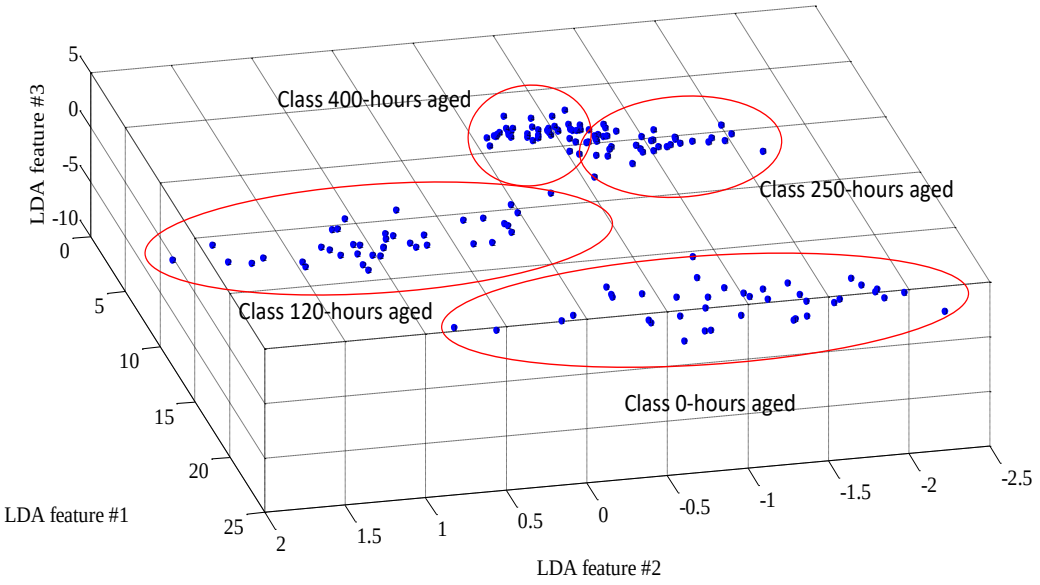

Fig. 5.7. Projection of $Energy$ Wavelet Transformed Features using LDA.

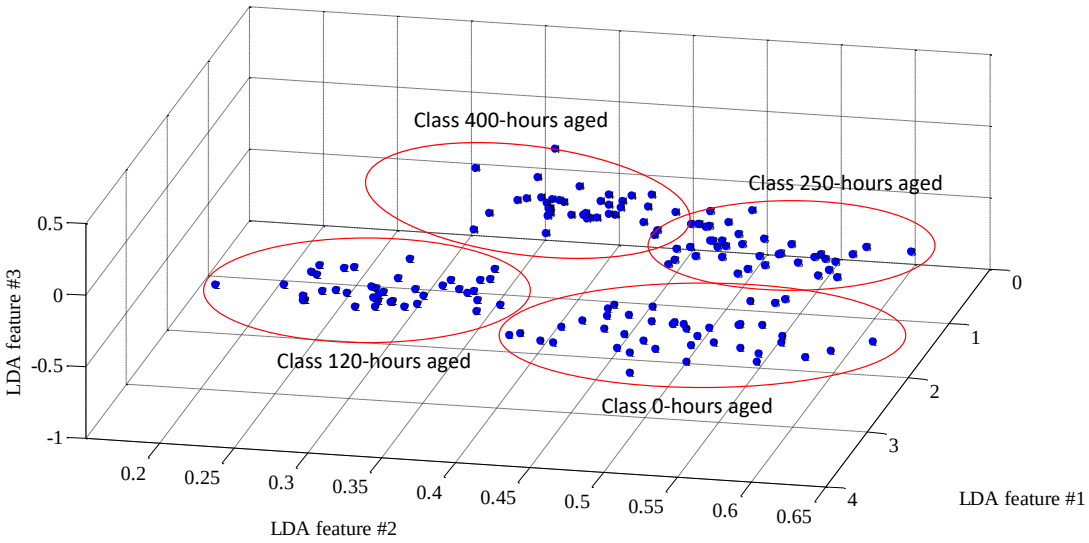

Fig. 5.8. Projection of $l1_{norm}$ Wavelet Transformed Features using LDA.

Table 5.3. Classification Error Summary for Wavelet Transform LDA and PCA classifiers from $l1_{norm}$ and $Energy$ Features

		Unseen Data Error Rate [%]	Cross Validation Error Rate [%]
l1-Norm	LDA	1.88	2.18
	PCA	1.25	3.49
Energy	LDA	3.13	3.49
	PCA	1.88	3.93

rates of 1.88% and 2.18%, respectively. These results are similar in performance to those obtained for the SGLDM texture analysis classifier in Table 4.3.

The PCA classifiers for $l1_{norm}$ and $energy$ features, reduce the original set of 12 Wavelet features per sample image to five PCA features. Five features are required to obtain a minimum of 95% variance from the original feature data set. Because the feature space is greater than three dimensions it is not possible to projections of the thermal deteriorated paper sample image data in the PCA feature space as was done for the LDA space in Fig. 5.7 and 5.8. Error rates for the $l1_{norm}$ and $energy$ PCA classifiers performed similarly well to the LDA classifier. The Wavelet $l1_{norm}$ PCA classifier yielded error rates of 1.25% for unseen data and 4.80% for cross-validation, while the $energy$ PCA classifier yielded error rates of 1.25% and 6.11% for unseen data and cross-validation respectively. Since PCA is an unsupervised learning method, the classifier training is carried out without knowing the class that each sample image belongs to. More than LDA, low error rates obtained for PCA classification suggest that the texture differences between paper samples from different aging classes are significant.

These results demonstrate that the Wavelet Texture Analysis method shows good promise for estimating level of deterioration in the samples aged at 0, 120, 250 and 400°C. These deterioration levels correspond to degree of polymerization values of 717, 316, 193, and 115 DP units respectively, which in a power transformer would correspond to new-condition, aged, at the threshold of end-of-life, and past end of life (high risk for failure).

5.3.4 Rotation Invariance Verification of the Classification Results

Because the Wavelet Texture features are orientation dependent, with detail coefficients computed in horizontal, vertical, and diagonal directions, it is needed to demonstrate that the texture features are rotationally invariant. If the microscopy images of the paper samples were obtained at different orientations in each class, this would influence the Wavelet classification because class differences may be due to the paper anisotropy and the computation of different features dependent on sample orientation. To demonstrate that the Wavelet Texture Analysis method in Section 5.2 is rotationally invariant, the classifier has been re-evaluated using features computed from randomly rotated sample images. In other words, the classifier was retrained with the same original training dataset except that prior to computation of the training features, the paper sample image was randomly rotated at angles in the range between -45° and +45°. Similarly, the 'unseen' or test samples were randomly rotated during classification and error evaluation. The classification error results calculated from the random rotation of paper sample images are shown in table 5.4.

5.4 Chapter Summary

Wavelet Transform analysis is a transform-based method of texture analysis. The images of thermally deteriorated paper samples are processed recursively in decompositions using the two dimensional Wavelet Transform. A total of four decompositions was performed, which yielded a total of 12 texture features obtained from the detail coefficient matrices at each

Table 5.4. Classification Summary Showing Verification of Rotational Invariance for Wavelet Transform LDA and PCA classifiers developed from randomly rotated sample images

		Unseen Data Error Rate [%]	Cross Validation Error Rate [%]
l1-Norm	LDA	1.25	3.93
	PCA	1.25	4.80
Energy	LDA	1.88	4.80
	PCA	1.25	6.11

decomposition level. Two feature sets were analyzed independently, one which computed the *energy* of the detail coefficients and another the $l1_{norm}$.

Analysis of the Wavelet texuture features showed that the fourth decomposition level yielded the greatest separation between aging classes. The average FDR between all class comparisons show and increasing trend with increasing decomposition levels between levels 1-4. Similar, to the SGLDM method, automated classification using supervised and unsupervised machine learning techniqes show low classification error rates. This again shows that the texture differences between aging classes are significant.

Chapter 6

Conclusions and Future Work

This research work has demonstrated that microscopy measurements from thermally deteriorated kraft paper can be analyzed using texture analysis methods to estimate the level of deterioration in power transformer paper insulation. An accelerated thermal aging experiment was developed and implemented to produce a set of kraft paper insulation samples that fall in to one of four coarse categories: new-condition paper, aged paper, end-of-life condition, and a condition that is beyond reliable operation end-of-life. Degree of polymerization measurements were used to confirm the aging level categories.

Microscopy measurements performed on the thermally deteriorated paper samples confirmed that with changes to mechanical properties of the paper that thermal deterioration also manifests as changes in the paper surface morphology. These morphological alterations to the paper surface were observed in microscopy measurements by the formation of cracks and fissures in the paper fibers, reductions in the paper fiber size, and distortions in the interwoven paper fiber network. Although similar observations about changes in the paper surface morphology have been made in previous work by other researchers, to the author's best knowledge this thesis research work is the first to attempt quantitatively analyze the surface morphology changes. Analysis was successfully carried out by the implementa-

tion of two different methods for texture analysis: a spatial grey level dependence method (SGLDM), and Wavelet texture analysis (WTA).

The SGLDM is a statistical based texture analysis method whereas the WTA is a transform based method. A main objective for this research was to apply texture analysis methods on microscopic images of the thermally deteriorated kraft insulation paper samples in order to characterize how the surface morphology changes as a function of thermal aging using texture analysis features. Sensitivity analysis of the texture features using Fisher Discriminant Ratios proved that discernible differences exist between aging classes. Correlation of the texture features with DP measurements showed that some texture features have a logarithmic relationship to DP. A significant finding from these results pertains to the SGLDM feature for entropy, which exhibits a similar relationship to DP as tensile strength. The results presented in this thesis show that the features developed from the SGLDM and the WTA trend proportionately with thermal deterioration, and that changes in the surface morphology are quantitatively related to tensile strength. This is a major finding and is counted as a main contribution in this thesis.

The second objective in this research was to explore integration of the texture features with machine learning techniques for automated classification of thermally deteriorated transformer insulation. The purpose of this objective is to evaluate the potential of microscopy and texture analysis as a method for condition assessment on power transformers. Results from applying supervised and unsupervised machine learning on the thermally aged paper samples demonstrated that deterioration level, falling into one of the four aging classes, is estimated with good accuracy. For the SGLDM method, the highest error rate obtained was 6.11% using an unsupervised learning algorithm (PCA). The fact that unsupervised learning yields a relatively low classification error indicates that the texture differences between aging classes are well separable. Using the LDA supervised learning classification method, the error rate is reduced to 3.49%. Similarly, Wavelet texture anal-

ysis results yield low error rates with an error of 3.93% and 3.49% for the PCA and the LDA classifiers respectively. These results demonstrate strong potential for the use of texture analysis on microscopic images of transformer paper insulation to estimate actual of deterioration level.

6.1 Future Work

With further development, this method demonstrates potential as an alternative to the established degree of polymerization test, however a larger body of experimental data is needed for the training of a robust classifier. Classification results based one paper type and thermal deterioration level belonging to one of the four coarse aging classes categorized as new-condition, mid-life, near end-of-life and beyond end-of-life are very promising and have low error rate. However, analysis of a much larger catalog of paper types from different manufacturers is required. Additionally, from the perspective of the asset (transformer) owner, greater precision is desired and therefore in future work, more samples should be prepared to aging levels that fall in-between the 0, 120, 250 and 400-hours that were used in this work. An analysis of actual in-service aged samples should also be performed in future work. The surface morphology of samples prepared in accelerated aging experiments may differ from those obtained from those aged in natural processes inside the transformer.

Potential benefits for this method over the degree of polymerization test are that the sample size required for analysis may be reduced and that the samples may be analyzed more quickly when factoring for time required to send paper samples to a chemical lab to have the degree of polymerization test performed. A long term objective in this research is for development of a reliable method of *in-situ* assessment on power transformer cellulose insulation that would not require removal of a physical paper sample. The design of an optical measurement arrangement suitable for *in-situ* measurement within a power transformer presents a major challenge. Such a method would allow for measurements to be

taken within the transformer tank during maintenance; while the transformer is off-line and drained of oil. Factors such as consistent illumination, image stabilization, and incident angle for imaging during measurement would have to be carefully considered for in-situ measurement, along with the health and safety of workers. The optical microscopy method used in this work has shown that texture analysis methods are very sensitive to the sharpness of focus that the images are captured with. Great care is required during the capture of microscopy images in order to ensure that they are in-focus for a majority of the image frame. Although portable microscopes exist that would be suitable for the application of in-situ measurement it, is anticipated that in-situ microscopy measurements would be vulnerable to poor focus in images due to the contoured installation of winding insulation paper. In future work alternative imaging technologies may be implemented to capture images of the winding insulation paper surfaces. Confocal laser scanning microscopy [23] and optical coherence tomography (OCT) may be considered as alternative imaging technologies for these measurements.

References

[1] H. P. Moser, *Transformerboard*. Scientia Electrica, 1979.

[2] *IEEE Guide for Loading Mineral-Oil-Immersed Transformers and Step-Voltage Regulators*, IEEE C57.91, 2012.

[3] I. Hohlein and A. J. Kachler, "Aging of cellulose at transformer service temperatures. part 2. influence of moisture and temperature on degree of polymerization and formation of furanic compounds in free-breathing systems," *IEEE Electrical Insulation Magazine*, vol. 21, no. 5, pp. 20–24, Sept 2005.

[4] D. Feng, *Life expectancy investigation of transmission power transformers*. The University of Manchester, Faculty of Electrical Engineering and Physical Sciences, 2013.

[5] L. Ruijin, T. Chao, Y. Lijun, and C. Huanchao, "Thermal aging studies on cellulose insulation paper of power transformer using afm," *8th International Conference on Properties and applications of Dielectric Materials*, pp. 722–725, June 2006.

[6] *Ageing of cellulose in mineral-oil insulated transformers*, Cigré Bulletin TB 323, Task Force D1.01.10, 2007.

[7] *IEEE Guide for the Interpretation of Gases Generated in Oil-Immersed Transformers*, IEEE C57.104-2008, 2009.

[8] *Standard Test Method for Measurement of Average Viscometric Degree of Polymerization of New and Aged Electrical Papers and Boards*, ASTM D4243-99, 2009.

[9] *Measurement of the average viscometric degree of polymerization of new and aged cellulosic electrically insulating materials*, IEC 60450, 2004.

[10] P. Verma, M. Roy, A. Verma, V. Bhanot, and O. Pandey, "Assessment of degradation of transformer insulation paper by sem and x-rd techniques," in *IEEE International Conference on Solid Dielectrics*, vol. 2, July 2004, pp. 657–660.

[11] L. Ruijin, T. Chao, Y. Lijun, and S. Gryzbowski, "Thermal aging micro-scale analysis of power transformer pressboard," *IEEE Transactions on Dielectrics and Insulation*, vol. 15, no. 5, pp. 1281–1287, October 2008.

[12] R. Haralick, K. Shanmugam, and I. Dinstein, "Textural features for image classification," *IEEE Transactions on Systems, Man and Cybernetics*, vol. SMC-3, no. 6, pp. 610–621, November 1973.

[13] G. Srinivasan and G. Shobha, "Statistical texture analysis," in *World Academy of Science, Engineering and Technology*, vol. 36, December 2008, pp. 1264–1269.

[14] T. Chang and C. C. J. Kuo, "Texture analysis and classification with tree-structured wavelet transform," *IEEE Transactions on Image Processing*, vol. 2, no. 4, pp. 429–441, Oct 1993.

[15] M. Popovic, "Texture analysis using 2d wavelet transform: theory and applications," in *Telecommunications in Modern Satellite, Cable and Broadcasting Services, 1999. 4th International Conference on*, vol. 1, 1999, pp. 149–158 vol.1.

[16] N. Jacob, D. Oliver, S. Sherif, and B. Kordi, "Classification of degradation in oil-impregnated cellulose insulation using texture analysis of optical microscopy images," *Electric Power Systems Research*, vol. 133, pp. 104–112, 2016.

[17] N. D. Jacob, D. R. Oliver, S. S. Sherif, and B. Kordi, "Statistical texture analysis of morphological changes in pressboard insulation due to thermal aging and partial discharges," in *2015 IEEE Electrical Insulation Conference (EIC)*, June 2015, pp. 610–613.

[18] N. Jacob, D. Oliver, S. Sherif, and B. Kordi, "Correlation of microscopic textural features and degree of polymerization for thermally deteriorated cellulose insulation," in *Proc. 2016 IEEE Electrical Insulation Conference*, June 2016.

[19] N. Jacob, B. Kordi, and S. Sherif, "Quantification of changes in surface texture of thermally-aged kraft paper using orthogonal wavelets," in *IEEE Electric Power and Energy Conference*, October 2017.

[20] A. A. Halacsy and G. H. V. Fuchs, "Transformer invented 75 years ago," *Transactions of the American Institute of Electrical Engineers. Part III: Power Apparatus and Systems*, vol. 80, no. 3, pp. 121–125, April 1961.

[21] T. A. Prevost and T. V. Oommen, "Cellulose insulation in oil-filled power transformers: Part i - history and development," *IEEE Electrical Insulation Magazine*, vol. 22, no. 1, pp. 28–35, Jan 2006.

[22] C. Krause, "Power transformer insulation history, technology and design," *IEEE Transactions on Dielectrics and Electrical Insulation*, vol. 19, no. 6, pp. 1941–1947, December 2012.

[23] J. Borch, M. B. Lyne, R. Mark, and C. Habeger, *Handbook of Physical Testing of Paper: Vol. 2.* Marcel Dekker Inc., 2002.

[24] W. Ziomek, K. Vijayan, D. Boyd, K. Kuby, and M. Franchek, "High voltage power transformer insulation design," in *2011 Electrical Insulation Conference (EIC).*, June 2011, pp. 211–215.

[25] T. Shugg, *Handbook of Electrical and Electronic Insulating Materials.* London: Van Nostrand Reinshold, 1986.

[26] T. A. Prevost, "Thermally upgraded insulation in transformers," in *Proceedings Electrical Insulation Conference and Electrical Manufacturing Expo, 2005.*, Oct 2005, pp. 120–125.

[27] "Tutorial on electrical grade papers in power transformers," *Doble Client Committee Fall Meeting*, October 1993.

[28] N. Lelekakis, J. Wijaya, D. Martin, and D. Susa, "The effect of acid accumulation in power-transformer oil on the aging rate of paper insulation," *IEEE Electrical Insulation Magazine*, vol. 30, no. 3, pp. 19–26, May 2014.

[29] K. S. Kassi, I. Fofana, F. Meghnefi, and Z. Yeo, "Impact of local overheating on conventional and hybrid insulations for power transformers," *IEEE Transactions on Dielectrics and Electrical Insulation*, vol. 22, no. 5, pp. 2543–2553, October 2015.

[30] A. Lokhanin, G. Shneider, V. Sokolov, V. Chornogotsky, and T. Morozova, "Internal insulation failure mechanisms of HV equipment under service conditions," *Cigre Report 15*, vol. 201, pp. 1–6, 2002.

[31] S. Chakravorti, D. Dey, and B. Chatterjee, *Recent Trends in the Condition Monitoring of Transformers.* London: Springer, 2013.

[32] M. Darveniza, T. K. Saha, D. J. T. Hill, and T. T. Le, "Investigations into effective methods for assessing the condition of insulation in aged power transformers," *IEEE Transactions on Power Delivery*, vol. 13, no. 4, pp. 1214–1223, Oct 1998.

[33] "Draft guide for dielectric frequency response test," *IEEE PC57.161/D2.0*, pp. 1–74, Jan 2017.

[34] M. F. M. Yousof, C. Ekanayake, and T. K. Saha, "Examining the ageing of transformer insulation using fra and fds techniques," *IEEE Transactions on Dielectrics and Electrical Insulation*, vol. 22, no. 2, pp. 1258–1265, April 2015.

[35] I. Hohlein and A. J. Kachler, "Aging of cellulose at transformer service temperatures. part 2. influence of moisture and temperature on degree of polymerization and formation of furanic compounds in free-breathing systems," *IEEE Electrical Insulation Magazine*, vol. 21, no. 5, pp. 20–24, Sept 2005.

[36] Susilo, Suwarno, U. Khayam, M. Tsuchie, M. Thein, M. Hikita, and T. Saito, "Study on dissolved gas due tue thermally degraded insulating paper in transformer oil," *Procedia Technology*, vol. 11, pp. 257 – 262, 2013.

[37] A. M. Emsley, X. Xiao, R. J. Heywood, and M. Ali, "Degradation of cellulosic insulation in power transformers. part 2: formation of furan products in insulating oil," *IEE Proceedings on Science Measurement and Technology*, vol. 147, no. 3, pp. 110–114, May 2000.

[38] *Mineral insulating oils - Methods for the determination of 2-furfural and related compounds*, IEC 61198, 1993.

[39] J. Jalbert, M. C. Lessard, and M. Ryadi, "Cellulose chemical markers in transformer oil insulation part 1: Temperature correction factors," *IEEE Transactions on Dielectrics and Electrical Insulation*, vol. 20, no. 6, pp. 2287–2291, December 2013.

[40] L. Cheim, D. Platts, T. Prevost, and S. Xu, "Furan analysis for liquid power transformers," *IEEE Electrical Insulation Magazine*, vol. 28, no. 2, pp. 8–21, March 2012.

[41] N. Azis, Q. Liu, and Z. D. Wang, "Ageing assessment of transformer paper insulation through post mortem analysis," *IEEE Transactions on Dielectrics and Electrical Insulation*, vol. 21, no. 2, pp. 845–853, April 2014.

[42] A. M. Emsley, R. J. Heywood, M. Ali, and X. Xiao, "Degradation of cellulosic insulation in power transformers .4. effects of ageing on the tensile strength of paper," *IEE Proceedings - Science, Measurement and Technology*, vol. 147, no. 6, pp. 285–290, Nov 2000.

[43] L. E. Lundgaard, W. Hansen, D. Linhjell, and T. J. Painter, "Aging of oil-impregnated paper in power transformers," *IEEE Transactions on Power Delivery*, vol. 19, no. 1, pp. 230–239, Jan 2004.

[44] P. Verma, D. Chauhan, and P. Singh, "Effects on tensile strength of transformer insulation paper under accelerated thermal and electrical stress," in *IEEE Conference on Electrical Insulation and Dielectric Phenomena*, Oct 2007, pp. 619–622.

[45] M. Karlovits and G. Gregor-Svetec, "Durability of cellulose and synthetic papers exposed to various methods of accelerated aging," *Acta Polytechnica Hungarica*, vol. 9, no. 6, pp. 81–100, 2012.

[46] G. Piantanida, M. Bicchieri, and C. Coluzza, "Atomic force microscopy characterization of the ageing of pure cellulose paper," *Elsevier Polymer Science*, vol. 46, no. 26, pp. 12 313 – 12 321, 2005.

[47] E. dos Santos, A. Monteiro, S. Silva, W. Fragoso, C. Pasquini, and M. Pimentel, "Determination of degree of polymerization of insulating paper using near infrared spectroscopy and multivariate calibration," *Vibrational Spectroscopy*, vol. 52, no. 2, pp. 154 – 157, 2010.

[48] P. J. S. Baird, H. Herman, and G. C. Stevens, "Non-destructive and in-situ analysis of insulating materials in high-voltage power transformers," in *Proceedings of the 2004 IEEE International Conference on Solid Dielectrics, 2004. ICSD 2004.*, vol. 2, July 2004, pp. 719–722.

[49] P. Baird, H. Herman, and G. Stevens, "Non-destructive condition assessment of insulating materials in power transformers," in *Electrical Insulating Materials, 2005. (ISEIM 2005). Proceedings of 2005 International Symposium on*, vol. 2, June 2005, pp. 425–428 Vol. 2.

[50] P. Baird, H. Herman, and Stevens, "On site analysis of transformer paper insulation using portable spectroscopy for chemometric prediction of aged condition," vol. 15, no. 4, August 2008, pp. 1089–1099.

[51] H. Khakmardani, *Ageing Asssessment of Power Transformer Kraft Paper Insulation Using Optical Speckle.* University of Manitoba, Faculty of Electrical and Computer Engineering, 2014.

[52] I. H. Isenberg, "Pulp and paper microscopy," *Institute of Paper Chemistry*, 1967.

[53] "Image texture analysis: methods and comparisons," *Chemometrics and Intelligent Laboratory Systems*, vol. 72, no. 1, pp. 57–71, 2004.

[54] A. Dixit and N. P. Hegde, "Image texture analysis - survey," in *2013 Third International Conference on Advanced Computing and Communication Technologies (ACCT)*, April 2013, pp. 69–76.

[55] A. S. Aguado, *Feature Extraction and Image Processing for Computer Vision.* Academic Press, 2012, vol. 3rd ed.

[56] S. Livens, P. Scheunders, G. van de Wouwer, and D. V. Dyck, "Wavelets for texture analysis, an overview," in *1997 Sixth International Conference on Image Processing and Its Applications*, vol. 2, Jul 1997, pp. 581–585 vol.2.

[57] M. Pietikainen, *Texture Analysis In Machine Vision.* World Scientific, 2000, no. vol. 40.

[58] M. Pietikäinen and T. Ojala, *Texture Analysis in Industrial Applications.* Berlin, Heidelberg: Springer Berlin Heidelberg, 1996, pp. 337–359.

[59] I. Stoica, A. I. Barzic, C. Hulubei, and D. Timpu, "Statistical analysis on morphology development of some semialicyclic polyimides using atomic force microscopy," *Microscopy Research and Technique*, vol. 76, no. 5, pp. 503–513, 2013.

[60] M. Reis and A. Bauer, "Image-based classification of paper surface quality using wavelet texture analysis," *Computers and Chemical Engineering*, vol. 34, no. 12, pp. 2014 – 2021, 2010.

[61] H. Zhai, H. Huang, S. He, and W. Liu, "Rice paper classification study based on signal processing and statistical methods in image texture analysis," in *2014 IEEE/ACIS 13th International Conference on Computer and Information Science (ICIS)*, June 2014, pp. 189–194.

[62] *Electrical insulation systems - thermal evaluation of combined liquid and solid components - Part 2: Simplified Test*, IEC 62332-2, 2014.

[63] *Standard Test Method for Sealed Tube Chemical Compatibility Test*, ASTM D5642-09, 2009.

[64] J. Singh, S. Y., and V. P., "Review of different prorated models which detect the effect of accelerated stresses on power transformer insulation," *International Journal of Computer and Electrical Engineering*, vol. 2, no. 3, pp. 569–574, June 2010.

[65] E. L. Morrisson, "Evaluation of the thermal stability of electrical insulation paper," *IEEE Transactions on Electrical Insulation*, vol. 3, no. 3, pp. 76–82, August 1967.

[66] Y. Du, M. Zahn, B. C. Lesieutre, A. V. Mamishev, and S. R. Lindgren, "Moisture equilibrium in transformer paper-oil systems," *IEEE Electrical Insulation Magazine*, vol. 15, no. 1, pp. 11–20, Jan 1999.

[67] "Standard for general requirements for liquid-immersed distribution, power, and regulating transformers," *IEEE Std C57.12.00-2010*, pp. 1–70, Sept 2010.

[68] R. C. Gonzalez and R. E. Woods, *Digital Image Processing 2nd Edition.* Pearson Education, 2009.

[69] MATLAB, *version 7.10.0 (R2010a).* Natick, Massachusetts: The MathWorks Inc., 2010.

[70] E. Gonzalez, F. Bianconi, M. Alvarez, and S. Saetta, "Automatic characterization of the visual appearance of industrial materials through colour and texture analysis: An overview of methods and applications," *Advances in Optical Technologies*, vol. 2013, no. 503541, pp. 1–11, September 2013.

[71] R. Yeung, *Information Theory and Network Coding.* New York: Springer Link, 2008.

[72] R. Duda, P. Hart, and D. Stork, *Pattern Classification Second Edition.* John Wiley and Sons, 2001.

[73] T. K. Sarkar, C. Su, R. Adve, M. Salazar-Palma, L. Garcia-Castillo, and R. R. Boix, "A tutorial on wavelets from an electrical engineering perspective. i. discrete wavelet techniques," *IEEE Antennas and Propagation Magazine*, vol. 40, no. 5, pp. 49–68, Oct 1998.

[74] I. Daubechies, *Ten Lectures on Wavelets.* Philadelphia, PA, USA: Society for Industrial and Applied Mathematics, 1992.

[75] E. Kuffel, W. S. Zaengl, and J. Kuffel, *High Voltage Engineering Fundamentals 2nd Edition*. Elsevier Ltd., 2000.

[76] V. Sokolov, Z. Berler, and V. Rashkes, "Effective methods of assessment of insulation system conditions in power transformers: a view based on practical experience," in *Electrical Insulation Conference and Electrical Manufacturing & Coil Winding Conference, 1999. Proceedings*. IEEE, 1999, pp. 659–667.

[77] P. Mitchinson, P. Lewin, B. Strawbridge, and P. Jarman, "Tracking and surface discharge at the oil-pressboard interface," *IEEE Electrical Insulation Magazine*, vol. 26, no. 2, pp. 35–41, March-April 2010.

[78] "High-voltage test techniques - partial discharge measurements," *IEC 60270*, 2000.

[79] P. Hiemenz and T. Lodge, *Polymer Chemistry*. Boca Raton: CRC Press, 2007.

[80] S. Weissberg, R. Simha, and S. Rothman, "Viscosity of dilute and moderately concentrated polymer solutions," *Journal of Research of the National Bureau of Standards*, vol. 47, no. 4, pp. 298–314, September 1951.

[81] *Standard Test Method for Intrinsic Viscosity of Cellulose*, ASTM D1795-96, 2001.

Appendix A

Machine Learning Techniques

In this appendix, formulas for machine learning methods are reviewed. These methods are used in Chapters 4 and 5 to develop classifiers that are used for automated estimation of deterioration level in thermally aged kraft paper samples.

A.1 Linear Discriminant Analysis

Linear discriminant analysis is a machine learning algorithm that uses a supervised learning method to develop a classifier. This means that the classifier is trained with prior knowledge of the class that each sample (feature vector) belongs to. From the feature extraction performed on the sample images belonging to each thermal aging class a feature vector is obtained for each aging class: 0, 120, 250, and 400 hours.

Linear discriminant analysis is obtained from the feature data set by first computing two matrices called scattering matrices. The between-class scatter S_B given in (A.1) measures the variance of each independent class mean $\hat{x}$ feature vector about the global mean vector μ_C. The parameter n_i represents the class number. The within-class scatter S_W in (A.2) is equivalent to the sum of the covariances among all classes. It provides a matrix equivalent for the amount of variance in each class independently.

$$S_B = \sum_C n_i(\mu_C - \hat{x})(\mu_C - \hat{x})^T \tag{A.1}$$

$$S_W = \sum_C \sum_{i \epsilon C} (x_i - \mu_C)(x_i - \mu_C)^T \tag{A.2}$$

The final projection vector is then determined from the eigenvectors of the product between the between-class S_B and within-class scatter S_W matrices determined by (A.3).

$$W = eig\{S_W^{-1} \cdot S_B\} \tag{A.3}$$

By sorting the eigenvalues from (A.3) in descending order the corresponding eigenvectors will ordered in terms of class separation feature class separation from largest separation to smallest. The vectors represent a linear combination of the original feature set, and by using only a portion of the feature vectors, dimensionality reduction of the original feature set may be obtained.

A.2 Principal Component Analysis

Principal component analysis (PCA) is a machine learning algorithm that uses an unsupervised learning method to generate a classifier. This means that the classifier is trained without prior knowledge of the class that each sample (feature vector) belongs to. Instead PCA translates the original dataset on to a reduced feature space which maximizes the variance present in the original dataset.

If the original feature set is represented by X is normalized by subtracting its mean becomes $\hat{X}$ then the covariance matrix is computed by (A.4)

$$\Sigma = \hat{X} \cdot \hat{X}^T \tag{A.4}$$

The final projection vector consisting of principal components is determined from the eigenvectors of the covariance matrix (A.5).

$$W = eig\{\Sigma\} \tag{A.5}$$

By sorting the eigenvalues from (A.3) in descending order the corresponding eigenvectors will ordered in terms of maximum to minimum variance in the dataset. The vectors represent a linear combination of the original feature set, and in using a portion of the principal component vectors, dimensionality reduction of the original feature set may be obtained.

Appendix B

Texture Analysis of Pressboard Insulation Deterioration from Partial Discharges

This appendix will present results from microscopic statistical texture analysis performed on transformer pressboard insulation which has been subjected to surface tracking partial discharge (PD) experiments. Results from these experiments were published in a conference paper [17]. Similar to transformer winding insulation paper, the intention of these experiments was to observe and quantify morphological change occurring on transformer pressboard material surfaces as a consequence of electrical discharges. An experimental test arrangement consisting of a needle and bar electrode incident on oil-immersed pressboard sample was used to cause electrical deterioration. The same (SGLDM) statistical texture analysis method was used analyze microscopic images of the pressboard surface, and the statistical features were compared between pressboard surface areas subjected to surface tracking discharges versus those surfaces that were not in an attempt to quantify the morphological change. Note that the results has been relegated to an appendix and outside the

main body of work in this thesis because the results obtained are inconclusive.

B.1 Pressboard deterioration and failure mechanisms

Partial discharge (PD) is a phenomena where applying high-voltage across an insulation system causes localized breakdown or arcing across small voids inside that system, or alternatively tracking along insulation surfaces [75]. Over time, sustained PD activity will degrade the insulation level of the system and can cause eventual failure.

Within a power transformer PD can occur at various locations of the insulation system where high electric field stress exists. These high stress regions may include streamer discharges propagating into the oil from surfaces of the transformer winding, discharges between the primary and secondary windings, discharge between winding turns, inter-phase discharges, or as surface tracking discharges.

A complex deterioration mechanism which can lead to power transformer failures involves the formation of PD along pressboard barriers surfaces; these are sometimes referred to as creepage discharge [76]. The presence of such discharge may originate due to undissolved gas or high moisture content in the pressboard resulting in PD or due to a phenomena called static electrification where surface friction between the pressboard and oil circulated in the power transformer causes a build-up of static charge on pressboard surfaces [75]. This charge in addition to the internal electric field stresses can result in the formation of PD. Surface tracking PD is most likely to occur on pressboard barrier insulation near the end winding regions of the transformer winding. At this region of the insulation system the electric field stress may be higher and the electric field lines are likely to travel parallel to the pressboard surfaces.

Recurrent PD can lead to the formation of permanent carbon tracks on the pressboard surfaces thus reducing the electrical insulation level. As a result the risk of catastrophic failure during electrical transients such as lightning strike or switching surges is elevated.

Fig. B.1. Converter transformer failure where evidence of partial discharge activity found on barrier surface between two windings.

An example of a transformer failure attributed to creepage discharge on pressboard is shown in fig. B.1.

B.2 Pressboard Specimen Materials

The pressboard material used in surface tracking partial discharge experiments is called TIV Transformerboard manufactured by Weidmann Electrical Technology Inc. TIV Transformerboard is a pre-compressed unbleached kraft board with a dimpled pattern on its surface. The board is supplied in large sheets and measures 1 mm in thickness. The TIV pressboard dimpled cellulose based pressboard. Samples were prepared in approximate dimensions of 100 mm $\times$ 80 mm for electrical stressing followed by microscopy and texture analysis as described in section B.3.

B.3 Electrical stress experimental setup

The experimental test arrangement designed to produce high electric field stress tangentially along pressboard surfaces, leading to localized partial discharge, is shown in Fig. B.2. The arrangement consists of a needle and bar electrode installed on a pressboard surface while immersed in transformer insulating oil. The needle is stainless steel with a 20μm tip radius, the ground electrode is an aluminum bar (10mm X 10mm X 10mm). A similar test arrangement has been used in [77].

The arrangement is designed to produce high divergent electric fields at the need tip along the pressboard surface. This will lead to surface PD in the region between the needle tip and the ground electrode. Partial discharge activity is measured using a high-voltage coupling capacitor according to methods described in [78] for apparent charge narrow-band PD measurement. A gap length of 20mm and voltage of approximately 30-33kV was sufficient to produce recurrent PD exceeding 1000 pico-Coulombs; where a typical phase-

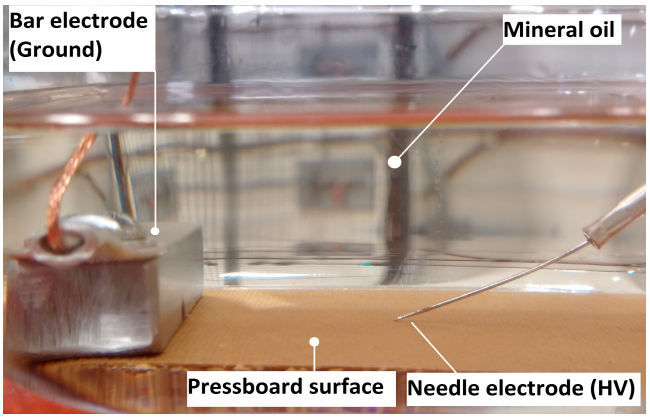

Fig. B.2. Surface tracking partial discharge test arrangement

resolved PD measurement is shown in fig.B.3. The number of hours for which samples will be electrically stressed will be varied to produce a sample set for optical analysis. Preliminary experiments performed thus far have shown that after four hours of electrical stress at 30kV physical changes on a pressboard sample surfaces appeared as shown in fig. B.4. Partial discharge causes gas channels to form in the pressboard surface. These gas channels are present only during testing and after the electrical stress is removed, the gas-channels are re-impregnated by the insulating oil and no longer visible. Carbon marks near the needle tip are permanent.

A test transformer was used to energize this arrangement and partial discharges measured using a 1000pF coupling capacitor along with an Omicron MPD Partial discharge measuring system. The applied voltage was increased to a level between 30-35kV on each of the pressboard samples. This was sufficient to produce regular discharges with pulse magnitudes greater than 1nC with repetition rates above 100 pulses-per-second. The samples subjected to electrical stress were exposed to 4-hours of surface PD. Following electrical stress, the samples were left in the oil for 24-hours at room temperature. These samples were then removed from the oil for microscopy imaging at 2.5X magnification. Twenty images were acquired from the pressboard region where surface discharges were active and

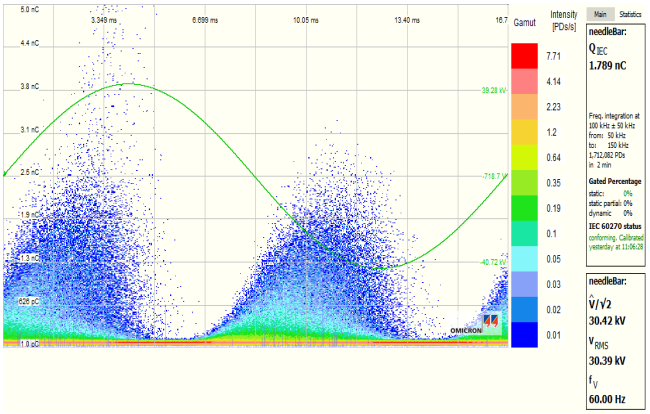

Fig. B.3. Typical phase-resolved PD plot obtained for pressboard surface discharges with needle-bar electrode arrangement.

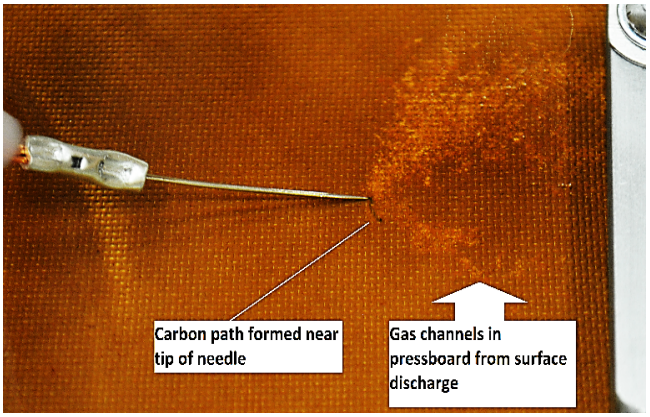

Fig. B.4. Electrical stress test arrangement produces gas channels in pressboard and carbon tracking marks.

twenty images from the regions with no surface discharge. The discharge region images were spread out over a general region between the electrodes but did not include carbonized regions where deterioration was visually obvious. Texture analysis by the SGLDM method described in 2.5 was performed on each aging class separately where the intent is to detect textural differences between the discharge regions versus the non-discharge regions of each sample.

B.4 Analysis of SGLDM features from surface tracking partial discharge

The SGLDM features obtained from microscopic images of electrically stressed pressboard are analyzed using Fisher discriminant ratios. This is procedure that was used for winding Kraft paper insulation in . Texture feature differences are measured between the region on the pressboard where surface tracking discharges occurred versus the non-discharge region. between features computed for the feature. The Fisher ratios for each SGLDM feature are shown in Table B.1. With all FDR less than one, this indicates that the morphological change in pressboard due to surface tracking PD is negligible. Comparatively, FDR values from pressboard samples subjected to surface tracking PD are considerably less than those obtained from thermally deteriorated paper samples in Table .

B.5 Appendix Summary

Based on the experiments performed for surface tracking PD deterioration of pressboard, results remain inconclusive. The change in texture features as a consequence of electrical deterioration are negligible as compared to those obtained from thermal deterioration of kraft winding insulation paper. It is anticipated that if surface tracking experiments would be prolonged that eventually texture differences would be perceptible and measurable using

Table B.1. Fisher Discriminant Ratio analysis of feature sensitivity comparison between the pressboard region having significant surface discharge versus region with no surface discharges.

Feature Name	Feature Number	FDR between discharge region and non-discharge region
Sum Variance	F6 & F17	0.995
Angular Second Moment	F1 & F12	0.709
Sum Entropy	F7 & F18	0.528
Sum Average	F5 & F16	0.513
Variance	F3 & F14	0.394
Entropy	F8 & F19	0.367
Inverse Difference Moment	F4 & F15	0.239
Information Measures of Correlation	F11 & F22	0.165
Difference Entropy	F10 & F21	0.079
Difference Variance	F9 & F20	0.040
Contrast	F2 & F13	0.015

this statistical texture analysis method. Presumably localized heat along with generation of gas channel in the pressboard that morphological changes would occur. This investigation is reserved for future work.

Appendix C

Description of the Average Viscometric Degree of Polymerization Test

The degree of polymerization of a particular cellulose molecule is equal to the number of glucose monomers units, $C_6H_{10}O_5$, which are connected in series, making up its molecular structure [8]. In a sample of paper the number of monomer units which make up individual cellulose molecules will vary. One common method used to estimate the average molecular weight of a polymer material involves measurement of the intrinsic viscosity of the material dissolved in a solution [79, 80]. Because intrinsic viscosity is related to polymer molecular weight, it is therefore related to average molecular length and the degree of polymerization in cellulose-based materials [81]. Empirical formulas which associate the degree of polmerization to intrinsic viscosity of a paper sample after it has been dissolved in a solution can be found in industry standards [8, 9].

This appendix provides a short description of the industry standard method used in [9] to determine the average viscometric degree of polymerization in plain electrical grade

papers used in power transformers, oil-paper insulated cables, and capacitors.

C.1 Sample Preparation

Preparation of paper samples is required prior to dissolution and viscosity measurement. Insulating oil impregnating the paper samples must be removed prior to dissolution because it would cause errors in the viscosity measurement otherwise. To remove oil, paper samples are cut into approximately $1mm^2$ sections. The oil content in the paper is removed by a process called Soxhlet extraction. In Soxhlet extraction, a solvent, either pentane or hexane, is percolated onto the paper sections which removes the oil. The samples are then left to dry and acclimatize to the laboratory ambient. Paper samples are then placed in a suitable blender or grinder to separate fibers and make for easier dissolution. The mass of dry paper m_D is measured.

For dissolution the dry separated paper is then placed in a solution which contains 50% distilled water and 50% solvent; called Cupriethylenediamine ($C_4H_{16}CuN_4$). Guidelines for the concentration and volume of the solvent to be used are given in [9] and is dependent on the mass of paper m_D and the expected condition of the paper. After the paper sample is fully dissolved the specific viscosity is measured.

C.2 Viscosity Measurement and Calculation of Viscometric Degree of Polymerization

Kinematic viscosity is measured using an Ubbelohde viscometer where its flow rate is measured in mm^2/s. All flow rates are measured multiple times per dissolved sample and the efflux times must agree to within 1%. The viscosity is measured on the Cupriethylenediamine/water solution before and after paper samples are dissolved. From these separate

viscosity measurements the specific viscosity ν_s is determined by (C.1):

$$\nu_s = \frac{[viscosity \quad of \quad paper \quad solution] - [viscosity \quad of \quad solvent]}{[viscosity \quad of \quad solvent]} \tag{C.1}$$

Intrinsic viscosity is calculated using the specific viscosity by solving $[\nu]$ in the empirical formula in (C.2).

$$\nu_s = [\nu] \cdot 10^{k \cdot [\nu] \cdot c} \tag{C.2}$$

The parameter k in (C.2) is called Martin's constant; $k = 0.14$ for plain kraft papers. The parameter c is the concentration of the solution, dependent on the mass of the sample m_D and the volume of the solution:

$$c = \frac{m_D}{\nu_{H_2O} + \nu_{Cu}} \quad [g/dl], \tag{C.3}$$

with ν_{H_2O} and ν_{Cu} representing the volume of water and Cupriethylenediamine solvent respectively.

Finally, the viscometric degree of polymerization is computed using the empirical formula in (C.4). The constants K and α are called the Mark Houwink constants and are K=0.0075 and α=1 respectively for Kraft paper.

$$[\nu] = K \cdot (\overline{DP}_\nu)^\alpha \tag{C.4}$$